LETTER

LARGE glycans on dystroglycan function as a tunable matrix scaffold to prevent dystrophy

Matthew M. Goddeeris[1,2], Biming Wu[1,2]†, David Venzke[1,2], Takako Yoshida-Moriguchi[1,2], Fumiaki Saito[3], Kiichiro Matsumura[3], Steven A. Moore[4] & Kevin P. Campbell[1,2,5,6]

The dense glycan coat that surrounds every cell is essential for cellular development and physiological function[1], and it is becoming appreciated that its composition is highly dynamic. Post-translational addition of the polysaccharide repeating unit [-3-xylose-α1,3-glucuronic acid-β1-]$_n$ by like-acetylglucosaminyltransferase (LARGE) is required for the glycoprotein dystroglycan to function as a receptor for proteins in the extracellular matrix[2,3]. Reductions in the amount of [-3-xylose-α1,3-glucuronic acid-β1-]$_n$ (hereafter referred to as LARGE-glycan) on dystroglycan result in heterogeneous forms of muscular dystrophy[4]. However, neither patient nor mouse studies has revealed a clear correlation between glycosylation status and phenotype[5,6]. This disparity can be attributed to our lack of knowledge of the cellular function of the LARGE-glycan repeat. Here we show that coordinated upregulation of *Large* and dystroglycan in differentiating mouse muscle facilitates rapid extension of LARGE-glycan repeat chains. Using synthesized LARGE-glycan repeats we show a direct correlation between LARGE-glycan extension and its binding capacity for extracellular matrix ligands. Blocking *Large* upregulation during muscle regeneration results in the synthesis of dystroglycan with minimal LARGE-glycan repeats in association with a less compact basement membrane, immature neuromuscular junctions and dysfunctional muscle predisposed to dystrophy. This was consistent with the finding that patients with increased clinical severity of disease have fewer LARGE-glycan repeats. Our results reveal that the LARGE-glycan of dystroglycan serves as a tunable extracellular matrix protein scaffold, the extension of which is required for normal skeletal muscle function.

LARGE is a dual-function glycosyltransferase that adds a glycan repeat to the basement membrane receptor dystroglycan (DG). DG is comprised of a transmembrane β-subunit and a cell-surface-associated α-subunit—the LARGE-glycan is bound to the latter through a rare structure at the amino terminus of its mucin-like domain, a phosphorylated *O*-mannosyl glycan[7,8]. The LARGE-glycan binds, with high affinity, to laminin-G-domain-containing matrix proteins (including laminin, agrin, perlecan and neurexin[9–12]). These interactions can be directly competed by the antibody IIH6, which specifically recognizes the LARGE-glycan. The amount of LARGE-glycan repeat present on α-DG has remarkable variability—both developmental[13,14] and tissue-specific[15], as shown by marked differences in α-DG apparent molecular mass. Mutations in *LARGE*, the DG-encoding gene (*DAG1*), and several other genes involved in synthesizing the *O*-mannosyl glycan[16–22] result in a group of muscular dystrophies termed dystroglycanopathies. These disorders encompass a broad spectrum of severity, ranging from late adult onset with predominant weakness of proximal muscle groups to more severe forms that present at birth and sometimes include defects in brain and eye development. Features common to these disorders are reduced ligand binding by α-DG and reduced to absent IIH6 immunoreactivity. However, when a cohort of dystroglycanopathy biopsies was assessed for IIH6 immunoreactivity by microscopy a correlation between staining intensity and clinical severity was not found[5].

It has been proposed that α-DG has separable, currently unknown roles in developing and fully differentiated skeletal muscle[23,24]; this could explain some of the observed clinical heterogeneity among dystroglycanopathy patients. To address this possibility without interfering with α-DG during embryogenesis, we developed the *GT(ROSA)26Sor*$^{tm407(H1/tetO-RNAi:Large)}$ (hereafter called *Large*^{KD}) inducible mouse model, in which *Large* is knocked down systemically through RNA interference (RNAi) (Extended Data Fig. 1a, b). On a standard diet, heterozygotes are phenotypically indistinguishable from littermates and α-DG glycosylation is normal (Extended Data Fig. 1c, d). When doxycycline is introduced through the diet, however, *Large* transcription is downregulated and IIH6 immunoreactivity in skeletal muscle and elsewhere is lost (Fig. 1a, b). Skeletal muscle has an extraordinary capacity for regeneration, a process that involves triggering satellite cell differentiation into myoblasts, which then proliferate and undergo myogenesis. We designed an experiment to test the impact of disrupted α-DG on regeneration, comparing muscle formed with normal versus defective α-DG. Specifically, we used *Naja nigricollis* cardiotoxin snake venom (CTX) to induce regeneration in select muscles of otherwise healthy adult *Large*^{KD} mice, and simultaneously began *Large* knockdown (Fig. 1c). Although β-DG was preserved in *Large*^{KD} muscle through 3 months after induction, LARGE-glycan was nearly eliminated (Fig. 1d). Gross analysis and quantification of multiple parameters in muscle from CTX-injected *Large*^{KD} mice and uninjected *Large*^{KD} and littermate controls (both CTX and uninjected) revealed that the test mice were profoundly dystrophic (Fig. 1d–g). Some uninjected *Large*^{KD} muscle myofibres featured centrally localized nuclei, indicating that the myofibre had previously regenerated, but evidence of active necrosis or regeneration (eMHC+ myofibres) was minimal despite the absence of LARGE-glycosylated α-DG. From these results we proposed that the degree to which a patient mutation affects α-DG LARGE glycosylation during muscle formation is a major determinant of disease severity.

Physiological assessment at earlier time points confirmed that LARGE-glycan is critical for muscle regeneration. Bilaterally CTX-injected *Large*^{KD} mice had significant deficits in downhill running within 3 weeks (Fig. 2a), whereas uninjected mice maintained running capacity in spite of a significant reduction in normally glycosylated α-DG (Extended Data Fig. 2a). Notably, *Large*^{KD} muscles recovering from CTX injury had abundant IIH6-positive α-DG, although of a reduced molecular mass (Fig. 2b and Extended Data Fig. 2a, b). Despite its low molecular mass, this α-DG was competent to bind laminin (Fig. 2b) and localized to the sarcolemma correctly (Fig. 2c). These results indicated that the number of α-DG LARGE-glycan repeats is critical to the cellular function of α-DG during muscle regeneration.

Histological examination of regenerating *Large*^{KD} muscles early after CTX treatment revealed that myofibres regenerate without a delay, but

[1]Howard Hughes Medical Institute, Roy J. and Lucille A. Carver College of Medicine, The University of Iowa, Iowa City, Iowa 52242, USA. [2]Department of Molecular Physiology and Biophysics, Roy J. and Lucille A. Carver College of Medicine, The University of Iowa, Iowa City, Iowa 52242, USA. [3]Department of Neurology and Neuroscience, Teikyo University School of Medicine, 2-11-1 Kaga, Itabashi-ku, Tokyo 173-8605, Japan. [4]Department of Pathology, Roy J. and Lucille A. Carver College of Medicine, The University of Iowa, Iowa City, Iowa 52242, USA. [5]Department of Neurology, Roy J. and Lucille A. Carver College of Medicine, The University of Iowa, Iowa City, Iowa 52242, USA. [6]Department of Internal Medicine, Roy J. and Lucille A. Carver College of Medicine, The University of Iowa, Iowa City, Iowa 52242, USA.
†Present address: Department of Biomedical Engineering, University of Michigan, Ann Arbor, Michigan 48109, USA.

Figure 1 | Muscle generated during *Large* knockdown is predisposed to aggressive dystrophy. a, b, Quantification of *Large* mRNA expression in *Large^KD^* mice on doxycycline (dox) induction (*n* = 3 animals per group, 2 experimental replicates) (**a**), and western blot-based determination of LARGE glycosylation 3 months after shRNA induction, and in littermate controls (ctrl) and LARGE-null negative control (*myd*) (**b**). Each lane is a sample from an individual animal. **c,** Experimental outline. Six weeks after CTX injury and simultaneous induction of *Large* knockdown, the mice were housed in cages with exercise wheels to circumvent the typical sedentary behaviour of laboratory mice (grey bar). Two experimental replicates for all analysis. **d,** Representative images of IIH6 and β-DG reactivity in immunofluorescence- and haematoxylin-and-eosin (H&E)-stained sections (black arrows, centrally nucleated myofibres). **e–g,** Tibialis anterior muscle sections (4 sections/muscle) of control and *Large^KD^* mice (white and black bars, respectively, *Large^KD^* mouse, *n* = 3; control, *n* = 4 biological replicates) were assessed for: **e,** fibre diameter (interaction *P* < 0.001, ~2,000 fibres per group; diamonds represent mean fibre diameter); **f,** average regions of necrosis (interaction *P* = 0.057); and **g,** average number of recently regenerated, embryonic myosin-positive fibres (interaction *P* = 0.007). Error bars represent s.d. in **e**, and s.e.m. elsewhere. Post-hoc comparisons **P* < 0.05, ** *P* < 0.0001; NS, not significant; ND, not detected. Scale bars, 100 μm.
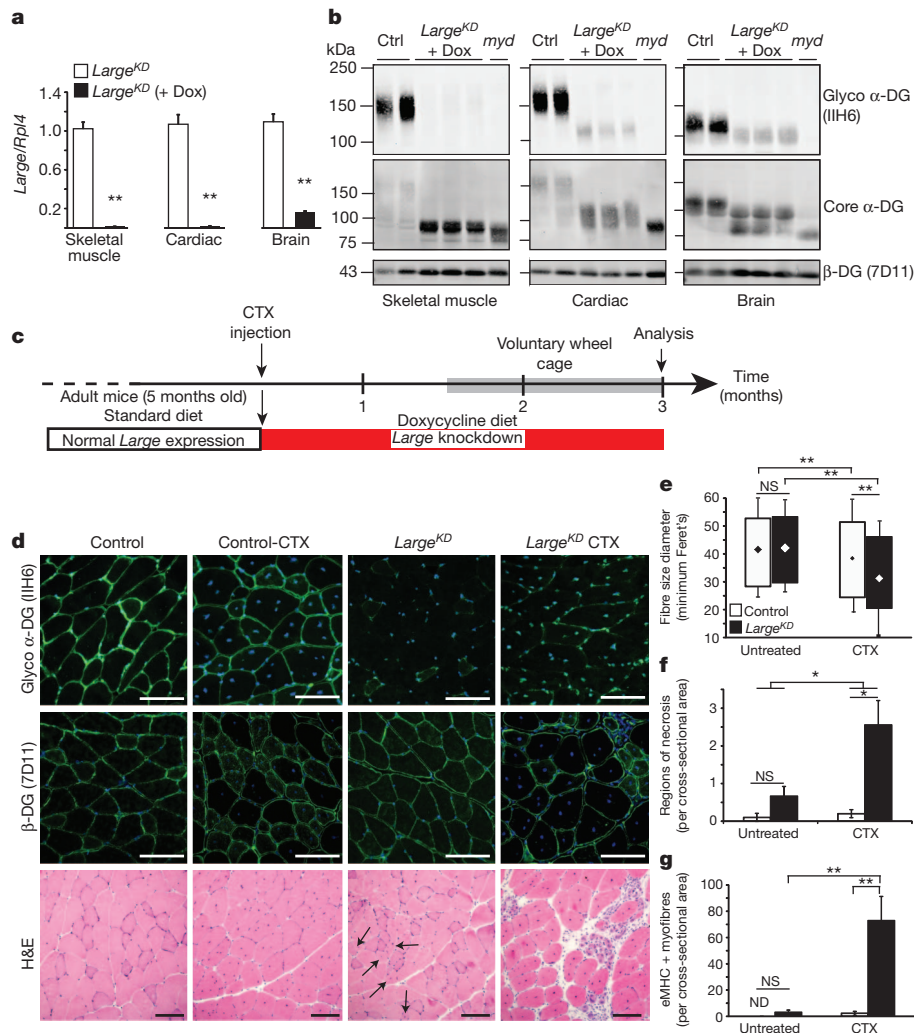
adipose cells, a feature commonly seen in severe muscular dystrophies, were observed (Extended Data Fig. 2c, d). Staining for perlecan, which normally co-localizes with laminin in the basement membrane, was reduced in intensity at the basement membrane but was also found mislocalized to the collagen-rich, extracellular matrix layer known as the endomysium (Extended Data Fig. 3a–e). Laminin α2 was similarly mislocalized to the endomysium (Extended Data Fig. 3f). Given that these findings were indicative of basement membrane abnormalities, we used transmission electron microscopy to probe for defects at the ultrastructural level. The presence of centrally localized nuclei, an increase in the presence of fibroblasts and macrophages, and an increase in the number of mitochondria at the myofibre periphery confirmed that the regions imaged had been damaged by CTX. In CTX-injected *Large^KD^* muscle, the basement membrane was significantly thickened and, unlike that in CTX control muscles, was often composed of multiple layers (Fig. 2d and Extended Data Fig. 3g). In addition to these abnormalities, collagen fibrils in the endomysial space were unusually abundant and often abnormally oriented with respect to the myofibres, consistent with the fibrous appearance of collagen structures by immunofluorescence (Extended Data Fig. 3a). The expression of collagen VI, perlecan and agrin was unaltered in CTX-injected *Large^KD^* muscles, although laminin isoforms were found to be elevated at both the mRNA and protein levels (Extended Data Fig. 4 and Fig. 2b). The observed layering of the basement membrane and the increase in thickness is consistent with reduced compaction of laminin and the collagen superstructures during basement membrane formation.

We next assessed the mechanism that underlies the variability in the molecular mass of α-DG. In regenerating control mice, α-DG shifts from approximately 100 kDa to 156 kDa (mode value) within 10 days of injury (Fig. 3a). This shift is closely paralleled by increases in the expression of basement membrane components laminin and collagen VI (Extended Data Fig. 5a), and by other biochemical hallmarks of regeneration such as a gradual loss of embryonic myosin and restoration of dihydropyridine receptor expression (Fig. 3a). To investigate such changes in greater detail we used the C2C12 mouse myoblast cell line, a classical model of myogenesis, which shows a marked increase in DG protein levels upon serum restriction[25]. The transition to larger glycoforms occurred rapidly after myoblasts are induced to differentiate, preceding myoblast fusion into myotubes on differentiation day (DD) 2 by 24 h (Fig. 3b and Extended Data Fig. 5b). The modal α-DG glycoform increased by 18 kDa over the course of the experiment (Extended Data Fig. 5c). This change correlated with rapid and sustained increases in *Large* and *Dag1* expression (Fig. 3c). Other modifiers of α-DG also showed increased expression levels but later and/or less acutely (Extended Data Fig. 6). We confirmed that other forms of α-DG glycosylation were not responsible for the increase in molecular mass, through enzymatic de-glycosylation removing the *N*-glycans, certain α-DG mucin *O*-glycans and terminal trisaccharides of *O*-mannosyl tetrasaccharides (a treatment that spares the phosphorylated *O*-mannosyl linked LARGE-glycan[7]). Notably, although both DD0 and DD4 α-DG migrated faster after de-glycosylation, the difference in molecular mass between the samples remained, as did the glycoform variation (band
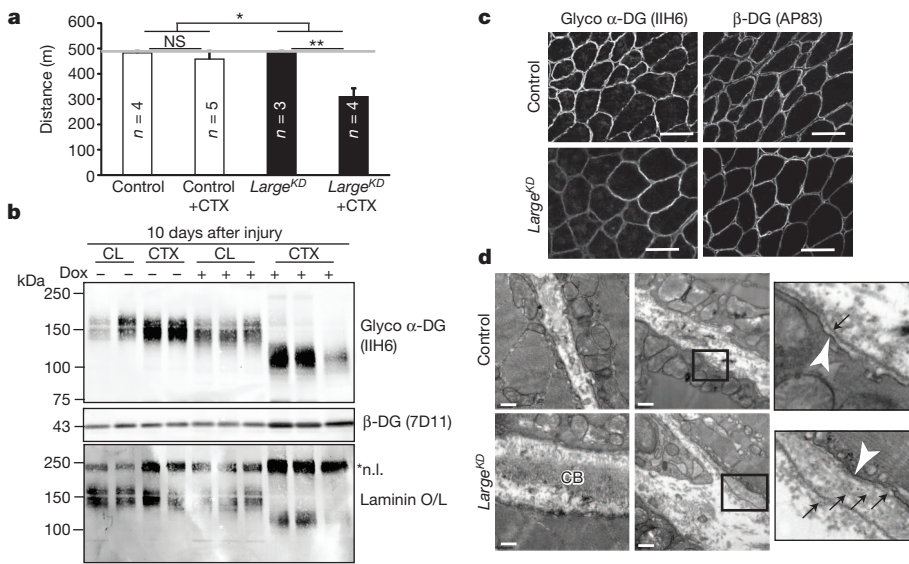
**Figure 2 | Regenerating *Large*[KD] muscle has α-DG of reduced molecular mass and basement membrane defects. a**, Quantification of muscle performance in downhill treadmill assay. Mice were injected bilaterally in the tibialis anterior and gastrocnemius muscles, and were given a 21-day recovery period. Grey line indicates predetermined assay end point (performance averages, interaction between genotype and CTX injury $P = 0.015$, post-hoc comparisons *$P < 0.05$, ** $P < 0.0001$, error bars indicate s.e.m., $n =$ biological replicate number for trial depicted, 3 experimental replicates). **b**, Western blot analysis and laminin overlay assay prepared from regenerating muscle, each lane representing an individual animal. CL, contralateral (un-injured) muscle; *n.l., native laminin. **c**, IIH6 and β-DG immunoreactivity of muscle sections. **d**, Muscle ultrastructure as assessed by transmission electron microscopy. White arrowhead, sarcolemma; black arrows, basement membrane; CB, collagen bundles. Samples in **b**–**d** were taken 10 days after CTX injury; scale bars, 50 μm (**c**) and 0.5 μm (**d**).

smearing) within each sample (Fig. 3d). We conclude that both inter- and intra-α-DG molecular mass variability during myogenesis is due to differences in the quantity of LARGE-glycan repeats. Next we measured inorganic phosphate chemically released from α-DG isolated from C2C12 DD1 (myoblasts) and DD5 (myotubes) after acid hydrolysis in conjunction with the malachite green phosphate assay. We found no significant difference (6.15 ± 2.37 μM versus 6.83 ± 2.19 μM phosphate released per unit DG for DD1 and DD5, respectively, $n = 3$ trials). Thus, the increase in α-DG LARGE-glycan content during

myogenesis is not attributable to the addition of new LARGE-glycan chains, but rather a consequence of extension of the LARGE-glycan chains present.

We proposed that a reduction in the LARGE-glycan degree of polymerization results in α-DG with reduced ligand-binding capacity. Using synthesized LARGE-glycan chains of either low (up to 13 repeats) or high molecular mass (>13 repeats) immobilized on ELISA assay plates, we performed binding assays for laminin, IIH6 and the perlecan V domain (Fig. 3e, f and Extended Data Fig. 7a–c). Binding to
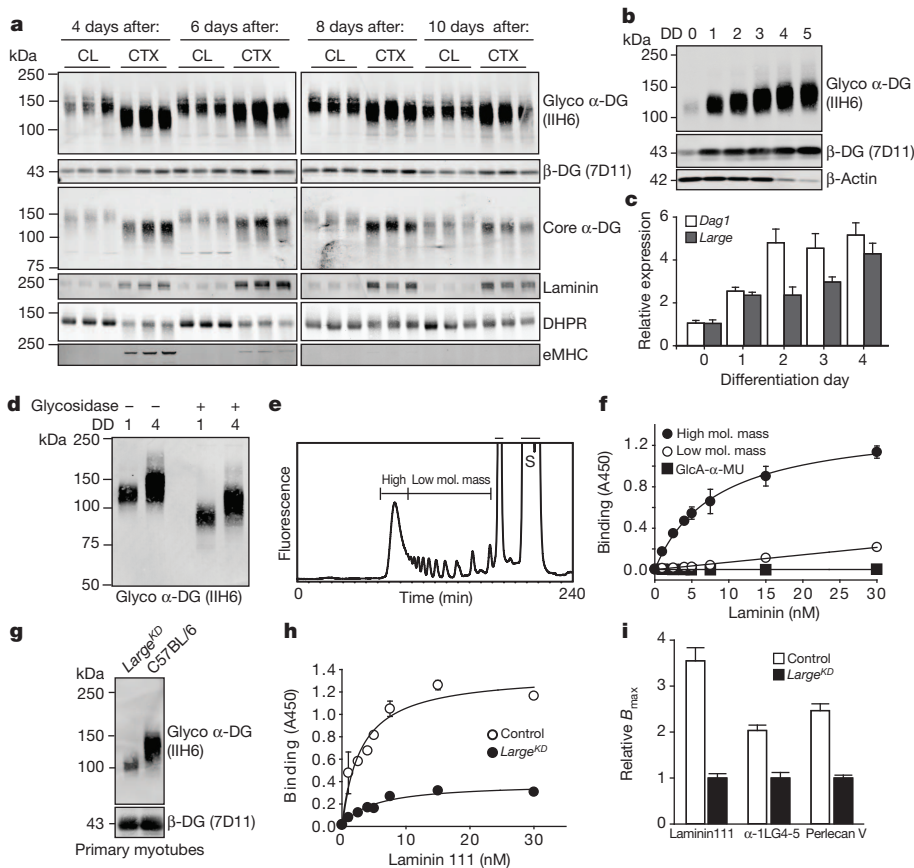
Figure 3 | Increase in α-DG LARGE-glycan chain length during myogenesis enhances ligand-binding capacity. a, Western blot analysis of WGA-enriched samples for expression of DG and other proteins at multiple times after CTX-mediated injury to C57BL6/J mice, each lane representing an individual animal. **b**, Western blot analysis of WGA-enriched lysates from C2C12 myoblasts undergoing myogenesis for functional α-DG (DD, differentiation day). At DD4–5 the loading control, β-actin, is downregulated in myotubes. **c**, qPCR analysis of *Dag1* and *Large* during C2C12 myogenesis (averages reported, $P < 0.001$, $n = 3$ biological replicates, $n \geq 7$ technical replicates, relative to *Rpl4* expression, error bars indicate s.e.m.). **d**, Western blot demonstrating effects of enzymatic de-glycosylation of DD0 and DD4 C2C12 protein samples. **e**, **f**, Elution profile of LARGE-glycan repeats on a gel filtration column. Bars indicate the fractions that were collected as the high- and low-molecular-mass LARGE repeats (S, substrate) used for solid-phase laminin 111 (**f**, high molecular mass $K_d = 8.2$) binding. **g**, DG western blot in DD4 myotubes from *Large*[KD] (+1 μg ml⁻¹ doxycycline) and control cultures. **h**, Solid-phase laminin 111 binding demonstrating that binding capacity is dependent on extension of the LARGE-glycan (control $K_d = 2.93 ± 0.776$ nM; *Large*[KD] $K_d = 4.75 ± 1.24$ nM). **i**, Comparison of solid-phase determined relative B_{max} values for several α-DG ligands (averages represented, B_{max} values for *Large*[KD] were set to 1 to allow for direct comparisons; error bars indicate s.e.m.). For solid-phase assays (**f** and **h**), error bars indicate s.e.m., $n = 3$ technical replicates, curve fitting to equation $f = B_{max}*abs(x)/(K_d + abs(x))$.

the low-molecular-mass LARGE-glycan was limited compared to that for the high-molecular-mass LARGE-glycan. Next, myotubes generated from primary cultures of isolated control and $Large^{KD}$ satellite cells were collected for α-DG solid-phase binding assays (Fig. 3g). The binding capacity (relative B_{max}) of α-DG from the $Large^{KD}$ myotubes was reduced for multiple ligands, including recombinant α1LG4-5 (2.04-fold), the perlecan V domain (2.47-fold), and laminin 111 (3.55-fold); the latter also displayed a small reduction in dissociation constant (K_d) (Fig. 3h and Extended Data Fig. 7d–f, summarized in Fig. 3i). These data demonstrate that the degree of LARGE-glycan polymerization, and thus the molecular mass of α-DG, correlates directly with the ligand-binding capacity of α-DG.

We reasoned that extension of the LARGE-glycan repeat chain during regeneration increased ligand-binding capacity by providing a larger scaffold for basement membrane components. The neuromuscular junction (NMJ) contains a basement membrane especially rich in α-DG ligands. According to our hypothesis, this structure should be disrupted in $Large^{KD}$ mice. Analysis of mice by tail suspension was consistent with such NMJ abnormalities in regenerated muscles; $Large^{KD}$ mice subjected to CTX injections into the tibialis anterior and gastrocnemius muscles clasped their hind paws instead of splaying them outward as was typical for control mice (Fig. 4a). Furthermore, analysis of acetylcholine receptor (AChR) labelling in these mice 21 days after CTX damage revealed that the NMJs were fragmented and irregular in shape (Fig. 4b, c), consistent with impaired maturation at the ultrastructural level. Finally, in AChR aggregation assays in primary myotube cultures, the addition of agrin or agrin plus laminin 111 to the medium of control myotubes led to a stepwise increase in AChR aggregate number and size, as previously demonstrated[26], but these increases were absent in $Large^{KD}$ myotubes (Fig. 4d, e). These findings demonstrate that normal NMJ maturation requires a high degree of LARGE-glycan polymerization, and that in the absence of such extension ligand saturation occurs.

Our data demonstrate that LARGE-glycan extension is required for reformation of both normal NMJs and the basement membrane after injury. Moreover, they indicate that the degree of LARGE-glycan polymerization is temporally coordinated with muscle regeneration. We thus tested whether the presence of excess LARGE-glycan early during regeneration would be detrimental. The overexpression of $Large$ (in CAG-$Large$ transgenic mice) resulted in hyper-glycosylated muscle α-DG, both at steady state (muscles not subjected to CTX injury) and shortly after CTX-induced muscle injury (Extended Data Fig. 8a, b). Glycosidase treatment of wheat-germ-agglutinin-enriched samples indicated that off-target activity owing to $Large$ overexpression was unlikely (Extended Data Fig. 8c, d), although we cannot entirely exclude a small

degree of nonspecific LARGE activity. Regenerated CAG-$Large$ myofibres were reduced in diameter and cross-sectional area, and myofibre density was increased, indicative of a defect in myoblast fusion (Extended Data Fig. 8e–i). These data support the notion that the pace of increased LARGE-glycan polymerization is an important aspect of α-DG function during muscle regeneration.

We next assessed human muscle biopsies from several forms of muscular dystrophy. Samples from two broad classes of muscular dystrophy were examined: more severe congenital forms (early-childhood onset, impact on non-muscle organs; congenital muscular dystrophy (CMD)), and a less severe form (adult-onset, impacting proximal muscles to a greater extent; limb girdle muscular dystrophy 2I (LGMD2I)). We observed a reduction in the molecular mass of IIH6-positive α-DG in the congenital muscular dystrophy muscle only (Extended Data Fig. 9a); whereas very little IIH6-positive α-DG was observed in the LGMD2I samples, the residual protein present was of typical molecular mass and restricted (as assessed by immunofluorescence) to muscle regions undergoing regeneration (Extended Data Fig. 9b). These results are in accordance with a previous study[13]. Consistent with our findings from $Large^{KD}$ mice, mislocalization of perlecan to the endomysial space was observed only in biopsies where α-DG was of reduced molecular mass (Extended Data Fig. 9c, d). Despite the fact that endomysial fibrosis in the LGMD2I biopsy was extensive, perlecan localization was normal, that is, restricted to the basement membrane. These data suggest that the typical late onset of LGMD2I is caused by loss of functional α-DG in the context of normal basement membrane formation. A previous analysis demonstrated that IIH6-positive α-DG could be recovered with $LARGE$ overexpression in dystroglycanopathy cell lines[27]. In light of our results, we propose that in some dystroglycanopathies the native increase in $LARGE$ function during myogenesis provides sufficient LARGE-glycan during muscle regeneration to lessen the impact of certain disease-causing mutations. If true, this would mean that the degree to which LARGE-glycan polymerization is reduced during muscle regeneration is a critical determinant of clinical severity.

Our findings demonstrate that the LARGE-glycan repeat of α-DG is a tunable scaffold for extracellular matrix proteins, the restriction of which through $Large$ knockdown during muscle regeneration both reduces muscle physiological function and predisposes it to dystrophy. Whereas the lower molecular mass α-DG retains the ability to bind laminin, our data are consistent with it binding fewer ligands per α-DG protein. In addition to binding the laminin network of the basement membrane, the LARGE-glycan also binds agrin and perlecan, which are capable of binding laminin and collagen concurrently. We speculate that when sufficient LARGE-glycan is available, these collateral linkages facilitate compaction of the basement membrane layers
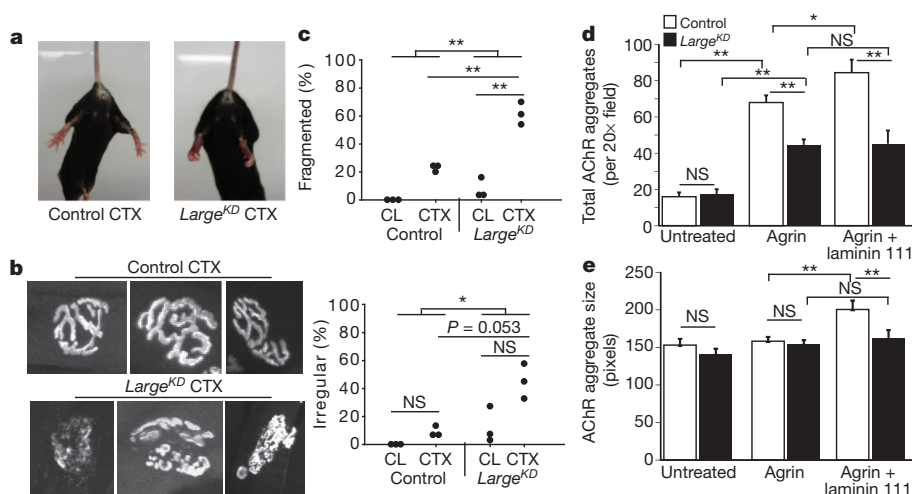
Figure 4 | **Reduction in α-DG LARGE-glycan chain length during myogenesis results in NMJ defects. a**, Hind-paw clasping phenotype during tail suspension in $Large^{KD}$ mice, 21 days after injury to the tibialis anterior and gastrocnemius muscles. **b**, Representative confocal images of AChR-labelled NMJs. **c**, Scoring of NMJ defects by blinded observers (scoring criteria in Methods, interaction $P = 0.011$ for fragmentation). **d, e**, Average AChR aggregation after ligand addition to control (white) or $Large^{KD}$ (black) DD4 myotubes (interaction $P < 0.001$ for total number and $P = 0.007$ for size; error bars indicate s.e.m.; ×20 magnification images, $n = 16$ per group). Post-hoc comparisons for **c–e** *$P < 0.05$, **$P < 0.0001$.

(Extended Data Fig. 10a, b). We also note that basement membranes from different tissues vary in both thickness and elasticity[28,29], and that α-DG is differentially glycosylated in a manner that affects ligand-binding characteristics (due mainly to differences in LARGE-glycan) across many tissues[15,30] (Extended Data Fig. 10c, d). It is thus possible that the capacity to fine-tune extension of the α-DG LARGE-glycan contributes to diversity in basement membrane structures across mammalian tissues.

METHODS SUMMARY

All mouse studies were performed on adult (8–15-week-old) mice raised on a standard mouse diet. 10 μM CTX (Accurate Chem & Sci Co in phosphate buffered saline) was used for intramuscular injections, at the following volumes: tibialis anterior, 25 μl; gastrocnemius, 50 μl. Injections of phosphate buffered saline alone did not cause observable muscle damage. Injections were unilateral unless otherwise noted. Mouse and human protein samples were processed similarly after 1% Triton X-100 solubilization of physically disrupted tissue. Glycoprotein enrichment via wheat-germ agglutinin (WGA) agarose beads (Vector Labs) was performed as described previously[9]. Induction of *Large* knockdown was achieved by replacing the normal mouse diet with equivalent chow containing 1 g kg^{-1} doxycycline (Bio-Serv) at the time of CTX injection.

Online Content Any additional Methods, Extended Data display items and Source Data are available in the online version of the paper; references unique to these sections appear only in the online paper.

1. Ohtsubo, K. & Marth, J. D. Glycosylation in cellular mechanisms of health and disease. *Cell* **126,** 855–867 (2006).
2. Inamori, K. *et al.* Dystroglycan function requires xylosyl- and glucuronyltransferase activities of LARGE. *Science* **335,** 93–96 (2012).
3. Kanagawa, M. *et al.* Molecular recognition by LARGE is essential for expression of functional dystroglycan. *Cell* **117,** 953–964 (2004).
4. Muntoni, F., Torelli, S., Wells, D. J. & Brown, S. C. Muscular dystrophies due to glycosylation defects: diagnosis and therapeutic strategies. *Curr. Opin. Neurol.* **24,** 437–442 (2011).
5. Jimenez-Mallebrera, C. *et al.* A comparative study of alpha-dystroglycan glycosylation in dystroglycanopathies suggests that the hypoglycosylation of alpha-dystroglycan does not consistently correlate with clinical severity. *Brain Pathol.* **19,** 596–611 (2009).
6. Kanagawa, M. *et al.* Residual laminin-binding activity and enhanced dystroglycan glycosylation by LARGE in novel model mice to dystroglycanopathy. *Hum. Mol. Genet.* **18,** 621–631 (2009).
7. Yoshida-Moriguchi, T. *et al.* O-mannosyl phosphorylation of alpha-dystroglycan is required for laminin binding. *Science* **327,** 88–92 (2010).
8. Hara, Y. *et al.* Like-acetylglucosaminyltransferase (LARGE)-dependent modification of dystroglycan at Thr-317/319 is required for laminin binding and arenavirus infection. *Proc. Natl Acad. Sci. USA* **108,** 17426–17431 (2011).
9. Michele, D. E. *et al.* Post-translational disruption of dystroglycan-ligand interactions in congenital muscular dystrophies. *Nature* **418,** 417–422 (2002).
10. Willer, T., Valero, M. C., Tanner, W., Cruces, J. & Strahl, S. O-mannosyl glycans: from yeast to novel associations with human disease. *Curr. Opin. Struct. Biol.* **13,** 621–630 (2003).
11. Barresi, R. *et al.* LARGE can functionally bypass α-dystroglycan glycosylation defects in distinct congenital muscular dystrophies. *Nature Med.* **10,** 696–703 (2004).
12. Sato, S. *et al.* Pikachurin, a dystroglycan ligand, is essential for photoreceptor ribbon synapse formation. *Nature Neurosci.* **11,** 923–931 (2008).
13. Brown, S. C. *et al.* Abnormalities in α-dystroglycan expression in MDC1C and LGMD2I muscular dystrophies. *Am. J. Pathol.* **164,** 727–737 (2004).
14. Leschziner, A. *et al.* Neural regulation of α-dystroglycan biosynthesis and glycosylation in skeletal muscle. *J. Neurochem.* **74,** 70–80 (2000).
15. Ibraghimov-Beskrovnaya, O. *et al.* Primary structure of dystrophin-associated glycoproteins linking dystrophin to the extracellular matrix. *Nature* **355,** 696–702 (1992).
16. Kobayashi, K. *et al.* An ancient retrotransposal insertion causes Fukuyama-type congenital muscular dystrophy. *Nature* **394,** 388–392 (1998).
17. Jurado, L. A., Coloma, A. & Cruces, J. Identification of a human homolog of the *Drosophila* rotated abdomen gene (POMT1) encoding a putative protein O-mannosyl-transferase, and assignment to human chromosome 9q34.1. *Genomics* **58,** 171–180 (1999).
18. Yoshida, A. *et al.* Muscular dystrophy and neuronal migration disorder caused by mutations in a glycosyltransferase, POMGnT1. *Dev. Cell* **1,** 717–724 (2001).
19. Brockington, M. *et al.* Mutations in the fukutin-related protein gene (FKRP) cause a form of congenital muscular dystrophy with secondary laminin α2 deficiency and abnormal glycosylation of α-dystroglycan. *Am. J. Hum. Genet.* **69,** 1198–1209 (2001).
20. Willer, T., Amselgruber, W., Deutzmann, R. & Strahl, S. Characterization of POMT2, a novel member of the PMT protein O-mannosyltransferase family specifically localized to the acrosome of mammalian spermatids. *Glycobiology* **12,** 771–783 (2002).
21. Longman, C. *et al.* Mutations in the human *LARGE* gene cause MDC1D, a novel form of congenital muscular dystrophy with severe mental retardation and abnormal glycosylation of α-dystroglycan. *Hum. Mol. Genet.* **12,** 2853–2861 (2003).
22. Willer, T. *et al.* ISPD loss-of-function mutations disrupt dystroglycan O-mannosylation and cause Walker-Warburg syndrome. *Nature Genet.* **44,** 575–580 (2012).
23. Cohn, R. D. *et al.* Disruption of DAG1 in differentiated skeletal muscle reveals a role for dystroglycan in muscle regeneration. *Cell* **110,** 639–648 (2002).
24. Beedle, A. M. *et al.* Mouse fukutin deletion impairs dystroglycan processing and recapitulates muscular dystrophy. *J. Clin. Invest.* **122,** 3330–3342 (2012).
25. Kostrominova, T. Y. & Tanzer, M. L. Temporal and spatial appearance of α-dystroglycan in differentiated mouse myoblasts in culture. *J. Cell. Biochem.* **58,** 527–534 (1995).
26. Montanaro, F. *et al.* Laminin and α-dystroglycan mediate acetylcholine receptor aggregation via a MuSK-independent pathway. *J. Neurosci.* **18,** 1250–1260 (1998).
27. Barresi, R. *et al.* LARGE can functionally bypass α-dystroglycan glycosylation defects in distinct congenital muscular dystrophies. *Nature Med.* **10,** 696–703 (2004).
28. Osawa, T., Onodera, M., Feng, X. Y. & Nozaka, Y. Comparison of the thickness of basement membranes in various tissues of the rat. *J. Electron Microsc.* **52,** 435–440 (2003).
29. Buxboim, A., Ivanovska, I. L. & Discher, D. E. Matrix elasticity, cytoskeletal forces and physics of the nucleus: how deeply do cells 'feel' outside and in? *J. Cell Sci.* **123,** 297–308 (2010).
30. Satz, J. S. *et al.* Distinct functions of glial and neuronal dystroglycan in the developing and adult mouse brain. *J. Neurosci.* **30,** 14560–14572 (2010).

Author Contributions M.M.G. co-designed the project, carried out the experimental work, analysed and interpreted the data and co-wrote the manuscript. B.W. conducted experimental work and analysed the data. D.V. generated essential reagents. T.Y.-M. generated LARGE-glycan repeat chains and performed binding assays thereon. F.S. and K.M. generated the *CAG-Large* transgenic mouse model. SA.M. compiled patient biopsies and edited the manuscript. K.P.C. co-designed the project, co-wrote the manuscript and supervised the research. All authors discussed the data and the manuscript.

Author Information Reprints and permissions information is available at www.nature.com/reprints. The authors declare no competing financial interests. Readers are welcome to comment on the online version of the paper. Correspondence and requests for materials should be addressed to K.P.C. (kevin-campbell@uowa.edu).

METHODS

Experimental replicates. Unless otherwise stated, all experiments were repeated in the laboratory three times. Data reported are representative.

Animals. Animal care, ethical usage and procedures were approved and performed in accordance with the standards set forth by the National Institutes of Health and the Animal Care Use and Review Committee at the University of Iowa. At the University of Iowa all mice are socially housed (unless single housing is required) under specific pathogen-free conditions in an AAALAC accredited animal facility. Housing conditions are as specified in the Guide for the Care and Use of Laboratory Animals (NRC). Mice are housed on Thoren brand, HEPA filtered ventilated racks, in solid bottom cages with mixed paper bedding. A standard 12/12-h light/dark cycle was used. Standard rodent chow (or special diet if required) and water is available ad libitum. C57BL6/J and *Large*^*myd* mice were obtained from The Jackson Laboratory. *Large*^*KD* mice were generated at TaconicArtemis GmbH. *CAG-Large* transgenics were generated by ligating a 1.7-kb fragment of the *CAG* promoter to a 2.3-kb fragment corresponding to positions +174 through +2444 of the *Large* (NM_010687) cDNA, plus the rabbit β-globin polyadenylation signal. The linearized 4.6-kb SalI-StuI *CAG-Large* construct was injected into pronuclei of fertilized zygotes from C57BL/6NTac mice and transferred to pseudopregnant females. Offspring were screened for genomic integration of this fragment by PCR of tail DNA, using the following *CAG-Large*-specific primers (PCR product size of 2.5 kb): forward 5′-CCTACAGCTCCTGGGCAACGTGCTGGTT-3′, reverse 5′-AGAGGGAAAAAGATCTCAGTGGTAT-3′. Mice were generated by breeding F$_1$ heterozygous transgenic males to wild-type females.

Mice were bred onto a C57BL6/J background (backcross 6 or greater). All mouse studies were performed on adult (8–15-week-old) mice raised on a standard mouse diet. Whereas within each experiment all subjects were sex- and age-matched (littermates where possible), both male and female mice were used and found to respond similarly with the exception of the downhill running assessment (Fig. 2a) wherein only male mice were used as performance variability was noted between the sexes. Previous experience with standard deviation of given techniques and pilot studies using naive animals were used to determine required power for experiments where appropriate with all efforts made to ensure animals for a given experiment were littermates or within 1 week of age. All treatment group designations (randomization) were assigned based on mice identification number and genotype information before experimenter's observation of the animals to exclude any bias based on animal appearance. 10 μM CTX (Accurate Chem & Sci Co) in phosphate buffered saline (PBS) was used for intramuscular injections, at the following volumes: tibialis anterior, 25 μl; gastrocnemius, 50 μl. Injections of PBS alone caused no observable muscle damage. Injections were unilateral unless otherwise noted. Induction of knockdown was achieved by replacing the normal mouse diet with an equivalent chow containing 1 g kg^{-1} doxycycline (Bio-Serv) at the time of CTX injection (day 0). Animals were exercised by downhill running (15° grade), using a variable speed belt treadmill (Omnipacer, AccuScan Instruments, Inc.) by an experimenter blinded to the genotypes of individual animals. Warm-up: 5 min, 3 metres per min (m.p.m.); running at the following paces; 10 m.p.m., 15 m.p.m., 20 m.p.m. for 5 min each, and 25 m.p.m. for 10 min or to exhaustion. Exhaustion was scored as 10 consecutive seconds of non-performance.

Human subjects and samples. Muscle biopsies were originally collected for diagnostic purposes and were obtained and tested according to the guidelines set out by the Human Subjects Institutional Review Board of the University of Iowa; informed consent was obtained from all subjects or their legal guardians.

Cell culture. C2C12 mouse myoblasts (freshly purchased from ATCC) were maintained in DMEM containing 10% FBS, 1% L-glutamine at 37 °C in 5% CO$_2$, and kept to a maximum of eight passages. For differentiation, cells were grown to confluence (designated differentiation day 0, DD0) and then switched to DMEM with 2% donor equine serum. AraC (cytosine β-D-arabinofuranoside hydrochloride, 10 nM final, Sigma) was added to differentiating C2C12 cells after myotubes formed, to limit the proliferation of differentiation-incompetent myoblasts. Satellite cell isolation was performed as per ref. 31. Satellite cells were plated on BD Matrigel-coated dishes and activated to differentiate into myoblasts in DMEM-F12, 20% fetal bovine serum (FBS), 40 ng ml^{-1} basic fibroblast growth factor (R&D Systems, 233-FB/CF), 1× non-essential amino acids, 0.14 mM β-mercaptoethanol, 1× penicillin/streptomycin and Fungizone. Myoblasts were maintained with 10 ng ml^{-1} basic fibroblast growth factor and differentiated in DMEM-F12, 2% FBS, 1× insulin-transferrin-selenium. For AChR-aggregation assays, primary myoblasts were seeded on BD Matrigel-coated glass coverslips.

Muscle analysis. Immunofluorescence and haematoxylin and eosin staining were carried out as described previously[9]. All images are representative from larger analysis of at least three animals per group, per condition. Fibre size diameter (minimal Feret's diameter) was assessed using ImageJ software (version 1.45s), based on β-DG immunofluorescence. Necrosis was assessed using anti-mouse IgG fluorescent antibody (detects immune-cell infiltration of degenerating fibres). qRT–PCR for mouse *Dag1* and associated glycosyltransferases was performed using a BioRad MyIQ system, with protocols and primer sets previously described[32]. The following primer sets were also used: *Ispd1* forward 5′-TGGTGTGGATTA GGGGGTTA-3′, reverse 5′-TGGCTGCACTTTGTCCTAAA-3′; *Tmem5* forward 5′-GAGAACAGTGGCAGCCTCA-3′, reverse 5′-CAAAGGAGCAGGCCTCAT AG-3′; *Sgk196* forward 5′-GCTGTCCTGTGAAGAGCTGA-3′, reverse 5′-GGG AGAGAGCGACTTTGTGT-3′; *Ignt1* forward 5′-ACATTTGACGAACGCTTTC-3′, reverse 5′-CCTCCTTTTGGGGATGGAAC-3′; *Itga7* forward 5′-TTGCTGTT AGCCACGATCAG-3′, reverse 5′-CGCCAGAGAAGAAGAGTTGC-3′; *Col6a* forward 5′-CTCTCCTGGTTCACCCATGT-3′, reverse 5′-CCCGACTCTACCG AGATTGA-3′; *Lama2* forward 5′-CCAAGAAGGAGGCTGCATAG-3′, reverse 5′-CCAGGTGTTGGGAAGACACT-3′; *Lamb1* forward 5′-GTTCGAGGGAAC TGCTTCTG-3′, reverse 5′-GTTCAGGCCTTTGGTGTTGT-3′; perlecan (*Hspg2*) forward 5′-GAGCGGACTGTACCTTGGTC-3′, reverse 5′-ACCAGTTGCACA CAGCTCAC-3′; agrin forward 5′-CAGTGGGGGACCTAGAAACA-3′, reverse 5′-ACCTTTCCAATCCACAGCAC-3′.

Fold changes were calculated using the ΔΔCt method. Failed reactions, those with Ct values within 1 Ct value of water control, were excluded. Mouse and human protein samples were obtained by 1% Triton X-100 solubilization of physically disrupted tissue. Glycoprotein enrichment via WGA agarose beads (Vector Labs) was performed as described previously[9]. Densitometry was performed using LiCor Odyssey Software, V3.0, of triplicate blots. Laminin overlay and solid-phase assays were performed as previously described[3,9]. For analysis of NMJs, Alexa-488-conjugated α-bungarotoxin was used to stain 4% paraformaldehyde-fixed tibialis anterior muscle cut into thirds longitudinally. Labelled muscle was cleared using glycerol and flattened. Maximal-intensity projections were obtained using an FV1000 Olympus Scanning Confocal laser microscope and z-stack sections compiled with FluoViewer-1.5 (Olympus). Next, individual NMJs from each image were assigned a number, cropped and copied onto a scoring PowerPoint file in a randomized fashion before scoring. Individual NMJs were scored by three blinded observers, using criteria established previously[33]. NMJs were scored as 'fragmented' if they were comprised of 5 or more AChR islands, and 'irregular" if they were abnormally shaped (either shallow folds and involutions or none at all). NMJs throughout the muscle were sampled, from 3 animals per group. *CAG-Large* mice were analysed for fibre size diameter (minimal Feret's), fibre cross-sectional area and density from images acquired using a VS120-S5-FL slide scanner microscope (Olympus) with VS-ASW (version 2.6). Analysis was carried out using VS-Desktop software version 2.6.

Statistics. All experimental data are representative of repeated experiments. Statistical analysis was performed using SigmaPlot software which determines if testing assumptions are met (Shapiro–Wilk normality and equal variance testing). Figure 1a used the Student's *t*-test, two sided. Figures 1e, f, 2a and 4c–e were analysed by two-way ANOVA. Post-hoc, pairwise multiple comparison procedures used the Holm–Sidak method with correction for multiple testing. Figure 3c data were analysed by one-way ANOVA on ranks.

Malachite green phosphate assay and sample preparation. C2C12 cells were differentiated on three 15-cm dishes and collected by physical scrapping. Cells were homogenized with 1% Triton X-100 by vortexing for 5 min, and insoluble material was centrifuged and discarded. An initial Lowry protein assay determined that starting protein was equivalent in each sample. DG pull-down was carried out using a β-DG-specific monoclonal antibody (8D5, Developmental Studies Hybridoma Bank) pre-bound to protein-A agarose beads (Santa Cruz Biotechnology). After extensive washing with 0.1% Triton X-100 in Tris-buffered saline, DG and the associated proteins were eluted using 0.1 M β-DG peptide. Samples were then dialysed exhaustively in ddH$_2$O (6,000–8,000 molecular mass cutoff, 5 days, 12+ 4 l changes). Concentrations relative to that of the α-DG core protein were determined by ELISA. Equal starting amounts of α-DG were then treated with 150 units calf intestinal alkaline phosphatase (CIP, New England Biolabs) for 30 min at 37 °C, to remove organic phosphate modifications such as the *O*-linked *N*,*N*′-diacetyllactosamine modification recently described for α-DG[34]. To release phosphate associated with the LARGE-glycan, samples were incubated with ice-cold 48% aqueous hydrofluoric acid at 0 °C for 20 h. The reagent was removed under a steady stream of nitrogen gas while on ice. Control samples were prepared by the same procedure, except that ice-cold water was used in place of hydrofluoric acid. Re-suspended samples were then assessed for phosphate content using the Malachite Green Phosphate Detection kit (R&D Systems).

LARGE-glycan preparation for the binding assays. 0.2 mM biotinylated GlcA-MU (custom synthesis by Sussex Research Laboratories Inc.) was incubated with LARGEdTM[7] 10 mM UDP-glucuronic acid (GlcA), 10 mM UDP-xylose (Xyl), 10 mM MgCl$_2$ and 10 mM MnCl$_2$ in 100 mM 2-(*N*-morpholino)ethanesulphonic acid (MES) buffer (pH 6.5) at 37 °C for 18 h. The enzymatic reaction was terminated by boiling in the presence of 50 mM EDTA. After centrifugation (20,000*g* for

10 min), the supernatant was fractionated using gel-filtration chromatography (Superdex peptide 10/300GL, GE Healthcare) as described previously[7]. The peaks eluted from retention time 75–97 min, and from 97–170 min were pooled as low-molecular-mass and high-molecular-mass LARGE repeats, respectively, and then lyophilized. The LARGE repeats in these two pools were dissolved in water and then analysed using a Bruker UltrafleXtreme MALDI-TOF/TOF mass spectrometer in negative reflection mode. α-Cyano-4-hydroxycinnamic acid (saturated in a mixture of acetonitrile and 0.1% TFA in 1:1 v/v) was used as the matrix as described[7]. To measure the concentration of MU-linked glycan, the glycan samples and known amounts of GlcA-MU were hydrolysed in 1 M of HCl at 95 °C for 20 min. The amounts of 4-methylumbelliferone released by acid hydrolysis were measured using a microplate reader Synergy4 (BioTek) (excitation, 350 nm; emission, 450 nm). GlcA-MU and low- and high-molecular-mass LARGE repeats (0.08 nmol per well) were immobilized on a NeutraAvidin coated 96-well plate (Pierce) according to the manufacturer's protocol. The plates were used for the solid-phase binding assays as described below.

Solid-phase binding assays. Myotube culture samples were collected by scraping and homogenized as described above. Total protein was quantified by Lowry protein assay, and equal amounts of protein were used to enrich for glycoproteins, using WGA agarose beads (Vector Labs) as described previously[9]. The use of equivalent amounts of DG was confirmed by ELISA to α-DG core protein and western blotting for β-DG. Samples were diluted with Tris-buffered saline 1:50, and bound to Costar 96-well, High Bind EIA/RIA plates (50 μl per well) overnight at 4 °C. Unbound sample was carefully aspirated and the plate blocked with 3% bovine serum albumin in laminin binding buffer (LBB; 746 mM triethanolamine, 140 mM NaCl, 1 mM CaCl$_2$, 1 mM MgCl$_2$, pH 7.6) for 2 h at room temperature. A series of ligand dilutions was prepared in LBB with a final concentration of 3% bovine serum albumin and 2 mM CaCl$_2$. Laminin 111 (Invitrogen), the perlecan V domain[35], the α1LG4-5 domain (isolated from conditioned medium from HEK293 cells secreting Flag-tagged α1LG4-5 domain, collected and enriched as described[36]), and AEBSF-laminin 111 were used in separate binding assays. To generate AEBSF-laminin 111, 10 mM serine protease inhibitor p-aminoethylbenzenesulphonyl fluoride AEBSF, HCl (Sigma) was incubated overnight on ice with 1 mg mouse laminin protein (Invitrogen) and used to inactivate laminin polymerization. AEBSF-treated laminin was dialysed to remove free AEBSF with 5 LBB changes of one litre each. Binding solutions were incubated with bound sample for 1 h at room temperature. Mixtures were aspirated completely and washed three times with 200 μl of 1% bovine serum albumin in LBB (wash solutions were aspirated each time). Primary antibodies to detect ligands were prepared in 3% bovine serum albumin in LBB and incubated for 1 h at room temperature. Antibody solutions were aspirated and washed before adding horseradish peroxidase conjugated secondary antibody (diluted in 3% bovine serum albumin in LBB) and incubating for 30 min at room temperature. After washing as before, sample reactions were developed using 100 μl pre-warmed 1-Step Ultra TMB-ELISA solution (Thermo Scientific) and stopped with 100 μl 2 M sulphuric acid. Absorbance was read at 450 nm, using a BioTek Synergy 4 microplate reader. For each ligand concentration, non-α-DG ligand binding was determined by blocking any LARGE-glycan bound to the plate with IIH6 antibody. The absorbance value from IIH6-blocked samples was subtracted from those of non-blocked samples to determine the specific binding activity of α-DG. Data from triplicate samples were assessed and fitted to a ligand-binding curve using SigmaPlot software. IIH6 ELISAs were completed similarly.

Tissue-specific α-DG ligand binding. Brains (cerebrum), hearts and quadriceps were collected from nine C57BL6/J male mice (9–10 weeks of age) and rinsed with ice-cold PBS. Samples were homogenized by Brinkmann Plytron (cardiac and skeletal muscle) or Wheaton Overhead Stirrer (brain) in 7.5 volumes of 20 mM sodium pyrophosphate, 20 mM sodium phosphate monobasic, 1 mM MgCl$_2$, 0.303 M sucrose, 0.5 M EDTA, pH 7.0. Samples were spun (15 min, 14,000g, 4 °C) and the supernatant was passed through cheesecloth to remove non-homogenized material. Total microsomes were obtained from the supernatant through ultra-centrifugation (37 min, 142,000g, 4 °C) and the microsomes were washed twice with 0.303 M sucrose, 0.6 M KCl, 20 mM Tris-maleate, pH 7.0 (recollecting microsomes by repeating ultra-centrifugation each wash) to remove loosely associated proteins. Total KCl washed microsomes were re-suspended in 0.303 M sucrose, 20 mM Tris-maleate, pH 7.0 and solubilized with 1% Triton X-100, 0.1% SDS. Non-solubilized material was removed by centrifugation (30 min, 30,000g, 4 °C) and the solubilized proteins (supernatant) were enriched for glycoproteins by WGA-agarose as described above. Equivalent loading for solid-phase binding assays was determined by preparing dilution curves and performing a β-DG ELISA assay. Solid-phase assays were performed as described above.

Glycosidase treatment. Treatment with glycosidases was as described previously[7], with sialidase (Prozyme) added to the Enzymatic Protein Deglycosylation kit (Sigma-Aldrich) containing: PNGaseF, O-glycosidase, β-N-acetylglucosaminidase,

β(1-4)-galactosidase. Glycosidase treatment was carried out on WGA-enriched total cell lysates after the native enzymes were heat inactivated (5 min incubation at 94 °C). Control (non-glycosidase treated) samples were treated identically without adding glycosidases.

AChR aggregation. The AChR aggregation assay was performed on DD4 myotubes differentiated on Matrigel-coated glass cover slides. Twelve hours before fixation, agrin (R&D Systems, 200 pM) and/or laminin 111 (7.5 nM) was added to the differentiation medium, to stimulate AChR aggregation. Samples were incubated for 30 min with Alexa-488-conjugated α-bungarotoxin (Invitrogen, 1:500), washed twice with cytoskeleton stabilizing buffer[37] (CSB) and fixed with 2% paraformaldehyde in CSB for 20 min at room temperature. Samples were blocked with 10% FBS, 0.3% Triton X-100 in PBS for 10 min and incubated overnight with IIH6 (1:50) and additional Alexa-488-conjugated α-bungarotoxin (1:1,000). Samples were imaged by confocal microscopy. Maximal intensity projections were obtained from confocal z-stacks and quantified using ImageJ software (version 1.45s).

Transmission electron microscopy. Tibialis anterior muscles were isolated from mice 10 days after CTX injection, after cardiac perfusion with PBS, and were treated with 4% paraformaldehyde in PBS. Samples were fixed in 2.5% glutaraldehyde, 2% paraformaldehyde, 1% tannic acid in 0.1 M Na cacodylate buffer (pH 7.3) for 1 h at 4 °C. They were then washed in 0.1 M Na cacodylate buffer and post-fixed with 1% osmium tetroxide for 1.5 h at 4 °C. After serial alcohol dehydration (50%, 75%, 95% and 100%), the tissue samples were embedded in Epon 12 (Ted Pella). Ultramicrotomy was performed, and ultrathin sections (65 nm) were post-stained with uranyl acetate and lead citrate. Samples were examined and imaged using a JEOL 1230 transmission electron microscope. Regions of interest, which had undergone regeneration due to CTX damage, were identified based on the presence of centrally localized nuclei and/or an accumulation of mitochondria at the sarcolemma.

Antibodies. The following antibodies have been described previously and were obtained from the listed sources: IIH6[38] monoclonal antibody (Campbell laboratory); monoclonal β-DG antibodies 8D5[39], MANDA G2 7D11[40] (Campbell laboratory); polyclonal anti-laminin (L9393) (Sigma-Aldrich); anti-Flag (Sigma-Aldrich); laminin-2 (α2 chain) 4H8-2 (Enzo Life Sciences); perlecan Ab-1 (NeoMarker); DHPR rabbit polyclonal antibody[41] to α2 subunit (Campbell laboratory); affinity purified β-DG rabbit polyclonal AP83[42] (Campbell laboratory); embryonic myosin heavy chain developed by H. Blau (F1.653, obtained from the Developmental Studies Hybridoma Bank under the auspices of the NICHD and maintained by The University of Iowa, Department of Biology); core α-DG antibody, RbtG6317[22] (Campbell laboratory); anti-collagen type VI (70R-CR009x, Fitzgerald Industries International); anti-β-actin (clone AC-74, Sigma-Aldrich); and anti-Flag antibody (F7425, Sigma-Aldrich).

31. Cerletti, M. et al. Highly efficient, functional engraftment of skeletal muscle stem cells in dystrophic muscles. Cell **134,** 37–47 (2008).
32. Groh, S. et al. Sarcoglycan complex: implications for metabolic defects in muscular dystrophies. J. Biol. Chem. **284,** 19178–19182 (2009).
33. Valdez, G. et al. Attenuation of age-related changes in mouse neuromuscular synapses by caloric restriction and exercise. Proc. Natl Acad. Sci. USA **107,** 14863–14868 (2010).
34. Breloy, I. et al. O-linked N,N′-diacetyllactosamine (LacdiNAc)-modified glycans in extracellular matrix glycoproteins are specifically phosphorylated at subterminal N-acetylglucosamine. J. Biol. Chem. **287,** 18275–18286 (2012).
35. Kanagawa, M. et al. Disruption of perlecan binding and matrix assembly by post-translational or genetic disruption of dystroglycan function. FEBS Lett. **579,** 4792–4796 (2005).
36. Harrison, D. et al. Crystal structure and cell surface anchorage sites of laminin α1LG4-5. J. Biol. Chem. **282,** 11573–11581 (2007).
37. Trendelenburg, A. U. et al. Myostatin reduces Akt/TORC1/p70S6K signaling, inhibiting myoblast differentiation and myotube size. Am. J. Physiol. Cell Physiol. **296,** C1258–C1270 (2009).
38. Ervasti, J. M., Ohlendieck, K., Kahl, S. D., Gaver, M. G. & Campbell, K. P. Deficiency of a glycoprotein component of the dystrophin complex in dystrophic muscle. Nature **345,** 315–319 (1990).
39. Masaki, T. et al. Expression of dystroglycan complex in satellite cells of dorsal root ganglia. Acta Neuropathol. **101,** 174–178 (2001).
40. Pereboev, A. V., Ahmed, N., thi Man, N. & Morris, G. E. Epitopes in the interacting regions of beta-dystroglycan (PPxY motif) and dystrophin (WW domain). Biochim. Biophys. Acta **1527,** 54–60 (2001).
41. Gurnett, C. A., Kahl, S. D., Anderson, R. D. & Campbell, K. P. Absence of the skeletal muscle sarcolemma chloride channel ClC-1 in myotonic mice. J. Biol. Chem. **270,** 9035–9038 (1995).
42. Williamson, R. A. et al. Dystroglycan is essential for early embryonic development: disruption of Reichert's membrane in Dag1-null mice. Hum. Mol. Genet. **6,** 831–841 (1997).
43. Hsu, N. Y. et al. Matrix-assisted laser desorption/ionization mass spectrometry of polysaccharides with 2′,4′,6′-trihydroxyacetophenone as matrix. Rapid Commun. Mass Spectrom. **21,** 2137–2146 (2007).

44. Colognato, H., Winkelmann, D. A. & Yurchenco, P. D. Laminin polymerization induces a receptor-cytoskeleton network. *J. Cell Biol.* **145,** 619–631 (1999).
45. Behrens, D. T. *et al.* The epidermal basement membrane is a composite of separate laminin- or collagen IV-containing networks connected by aggregated perlecan, but not by nidogens. *J. Biol. Chem.* **287,** 18700–18709 (2012).
46. Noakes, P. G., Gautam, M., Mudd, J., Sanes, J. R. & Merlie, J. P. Aberrant differentiation of neuromuscular junctions in mice lacking s-laminin/laminin β2. *Nature* **374,** 258–262 (1995).
47. Han, R. *et al.* Basal lamina strengthens cell membrane integrity via the laminin G domain-binding motif of α-dystroglycan. *Proc. Natl Acad. Sci. USA* **106,** 12573–12579 (2009).
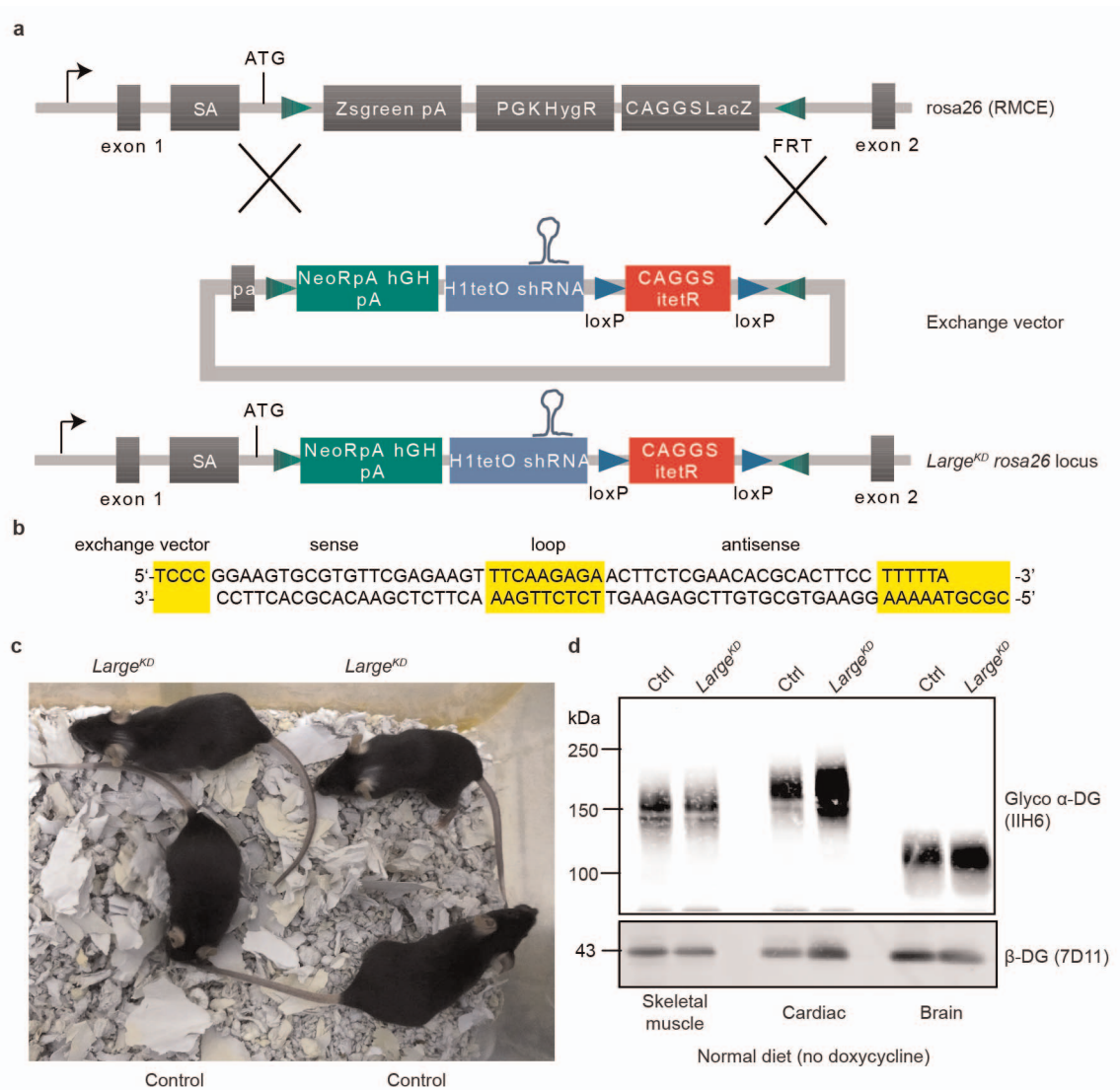
Extended Data Figure 1 | Generation of *Large^KD* mice.
a, *GT(ROSA)26Sor^tm407(H1/tetO-RNAi:Large)* (*Large^KD*)-targeted mice were generated at TaconicArtemis GmbH, using an engineered recombinase-mediated exchange acceptor site in the *Rosa26* gene, and an exchange vector with the following elements: a neomycin resistance marker; an H1-Tet-On promoter-driven shRNA that targets *Large*; and a *loxP*-flanked CAGGS promoter-driven Tet repressor. Mouse embryonic stem cells with the above-described *Rosa26* gene were exposed to six distinct doxycycline-inducible/conditional shRNA constructs that target *Large*. After validation for correct targeting by Southern blotting, the ES cells were evaluated for efficient *Large* knockdown by qPCR, and for functional loss of IIH6-positive α-DG by western blotting. One knockdown embryonic stem (ES) cell line (targeting the sequence: GGAAGTGCGTGTTCGAGAAGT) was selected for use in blastocyst injections to generate chimaeric mice, on the basis of the efficiency of *Large* knockdown efficiency therein. Germline animals heterozygous for the knockdown cassette were backcrossed onto a C57BL6/J background. **b**, shRNA sequence used to target *Large*. **c**, **d**, *Large^KD* mice and littermate controls. In the absence of doxycycline, the animals are indistinguishable from control littermates both phenotypically (**c**) and biochemically (**d**).
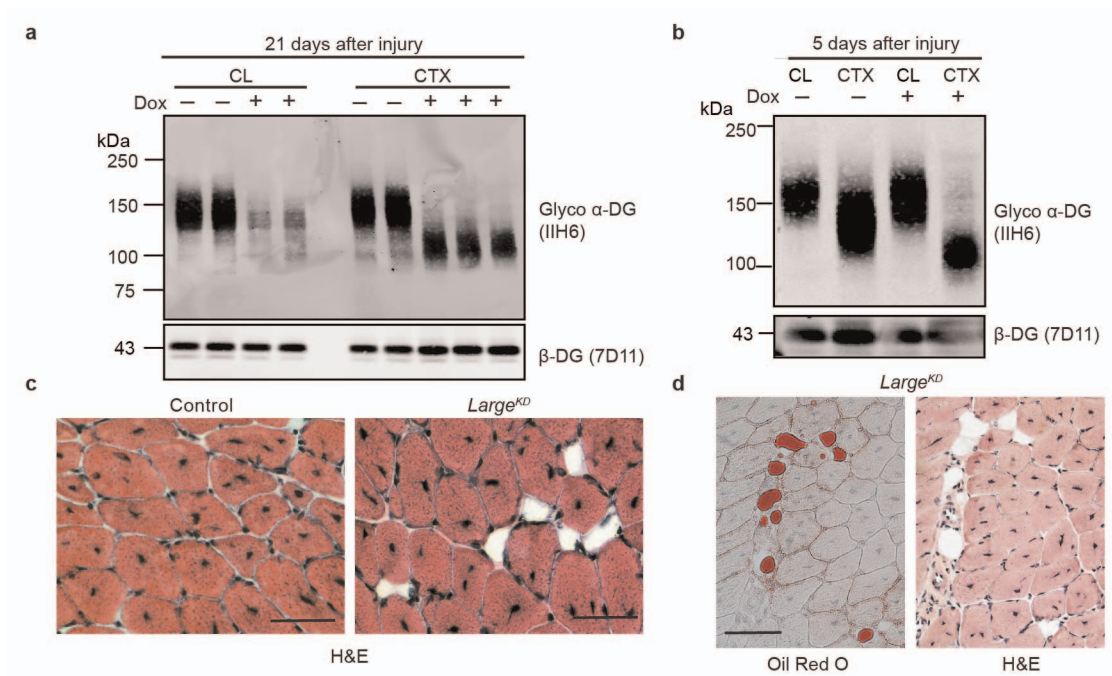
Extended Data Figure 2 | Reduction in molecular mass of α-DG during and after regeneration and increased adipose staining in *Large^KD* muscle.
a, b, Western blot analysis of WGA-enriched Triton X-100-soluble homogenates from the tibialis anterior muscles of *Large^KD* mice 21 (**a**) and 5 (**b**) days after CTX injury. Glycosylation of α-DG is 're-set' to a lower molecular mass in the *Large^KD* (dox+) mice. At 21 days after CTX injury, the contralateral (CL), uninjured *Large^KD* (dox+) muscle exhibits reduced IIH6 intensity relative to control (dox−), although the molecular mass in the two samples is

equivalent. In the 5-day samples, this reduction is not observed, a finding that indicates the loss of reactivity in the 21-day samples is attributable to loss of pre-existing α-DG and failure to replace with IIH6-positive α-DG owing to *Large* knockdown. At 5 days after injury, a marked increase in molecular mass variation is observed in CTX control tissue (similar to Fig. 3a). **c**, Haematoxylin and eosin (H&E) analysis reveals evidence of intramuscular adipose cells in *Large^KD* gastrocnemius muscle 10 days after CTX. **d**, Staining with the lipophilic dye Oil Red O, confirming that fat is present. Scale bars, 50 μm.
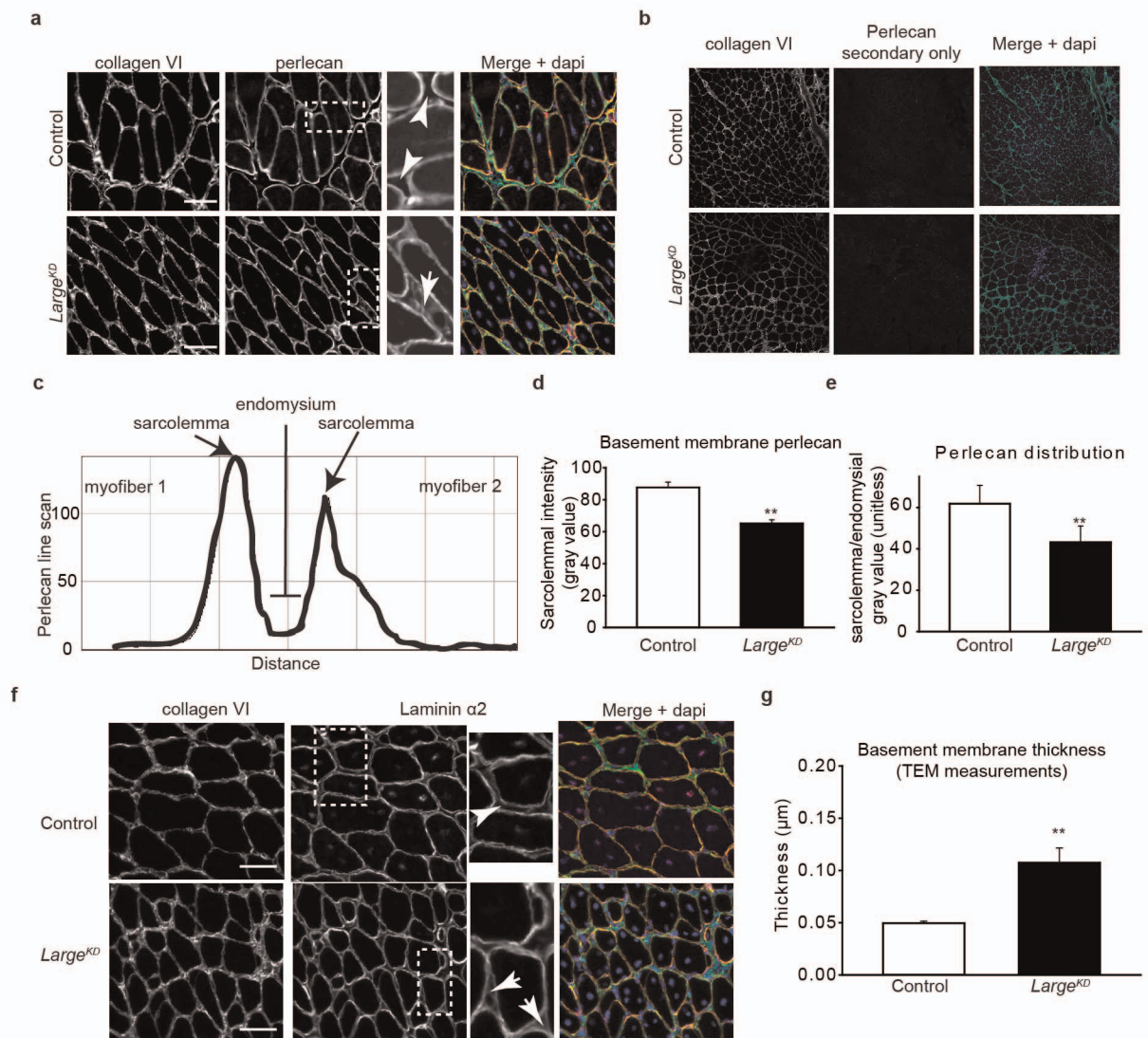
Extended Data Figure 3 | Basement membrane abnormalities in *Large^KD* muscle. *Large^KD* muscle at 10 days after CTX. **a**, Collagen VI and perlecan co-labelling of muscle sections. Arrowheads, lack of perlecan (normal) in endomysial space; arrow, perlecan in the endomysium. **b**, Secondary only control experiment demonstrating specificity of perlecan signal. **c**, Line scan intensity analysis for perlecan staining across adjacent myofibres, conducted by a blinded third-party. In the example shown (from a control muscle), increased sarcolemmal/basement membrane staining intensity is observed for the two adjacent myofibres, with minimal staining in the intervening endomysial space. Results of this analysis are quantified in **d**, **e**. For perlecan analysis eight line scans were conducted on at least three, ×20 images from 10-day post CTX injury muscles (*n* = 4 CTX injured mice per group). One-way ANOVA on ranks was used to assess the data. For **d** and **e**, **$P < 0.001$, error bars indicate s.e.m. **f**, Collagen VI, which is expressed during muscle regeneration, localizes to both the basement membrane and the endomysium in control and *Large^KD* muscle 10 days after CTX. Laminin α2, which is normally restricted to the basement membrane in control muscle, is also observed in the endomysium of *Large^KD* muscle (arrows). Arrowhead points to endomysium in control muscle. All images in **a**, **b** and **f** were collected with confocal microscopy, scale bars, 50 μm. **g**, Quantification of the increase in basement membrane thickness on the basis of transmission electron microscopy of muscle 10 days after CTX injury. Over six images from two *Large^KD* and three control animals were assessed by a blinded observer using ImageJ software. One-way ANOVA was used to assess the data; **$P = 0.001$, error bars indicate s.e.m.
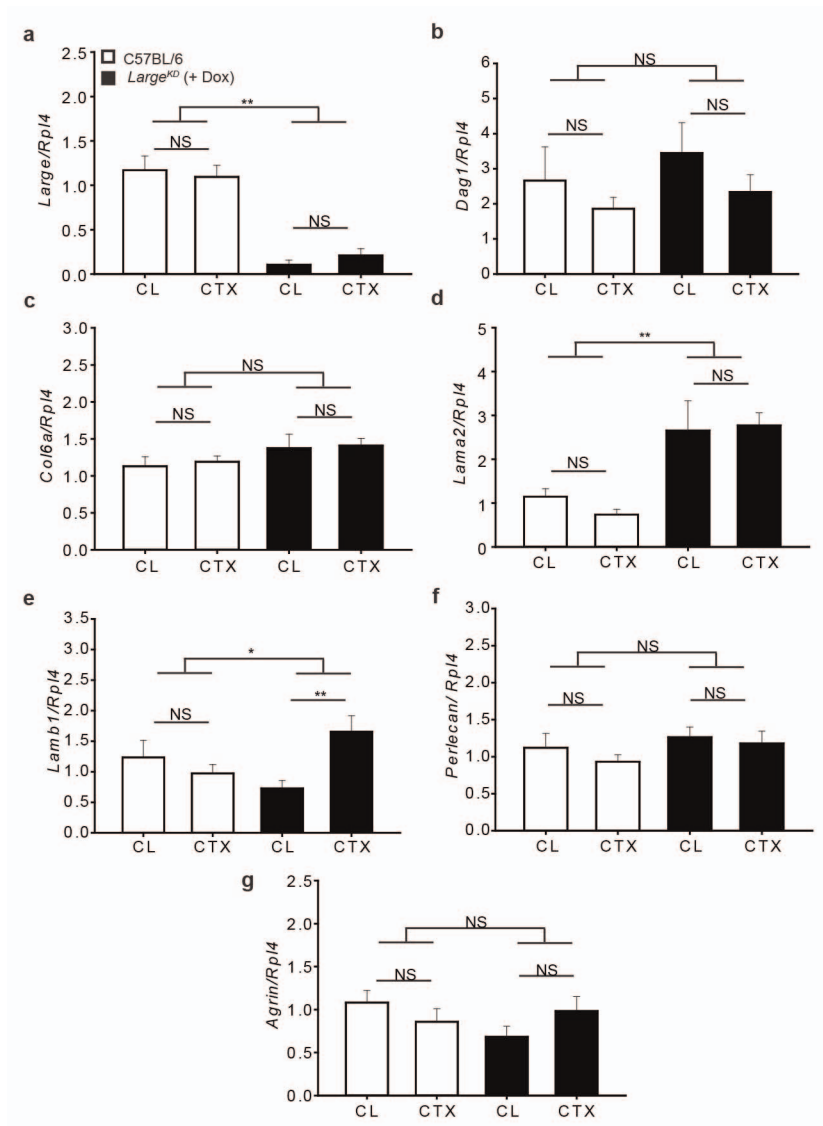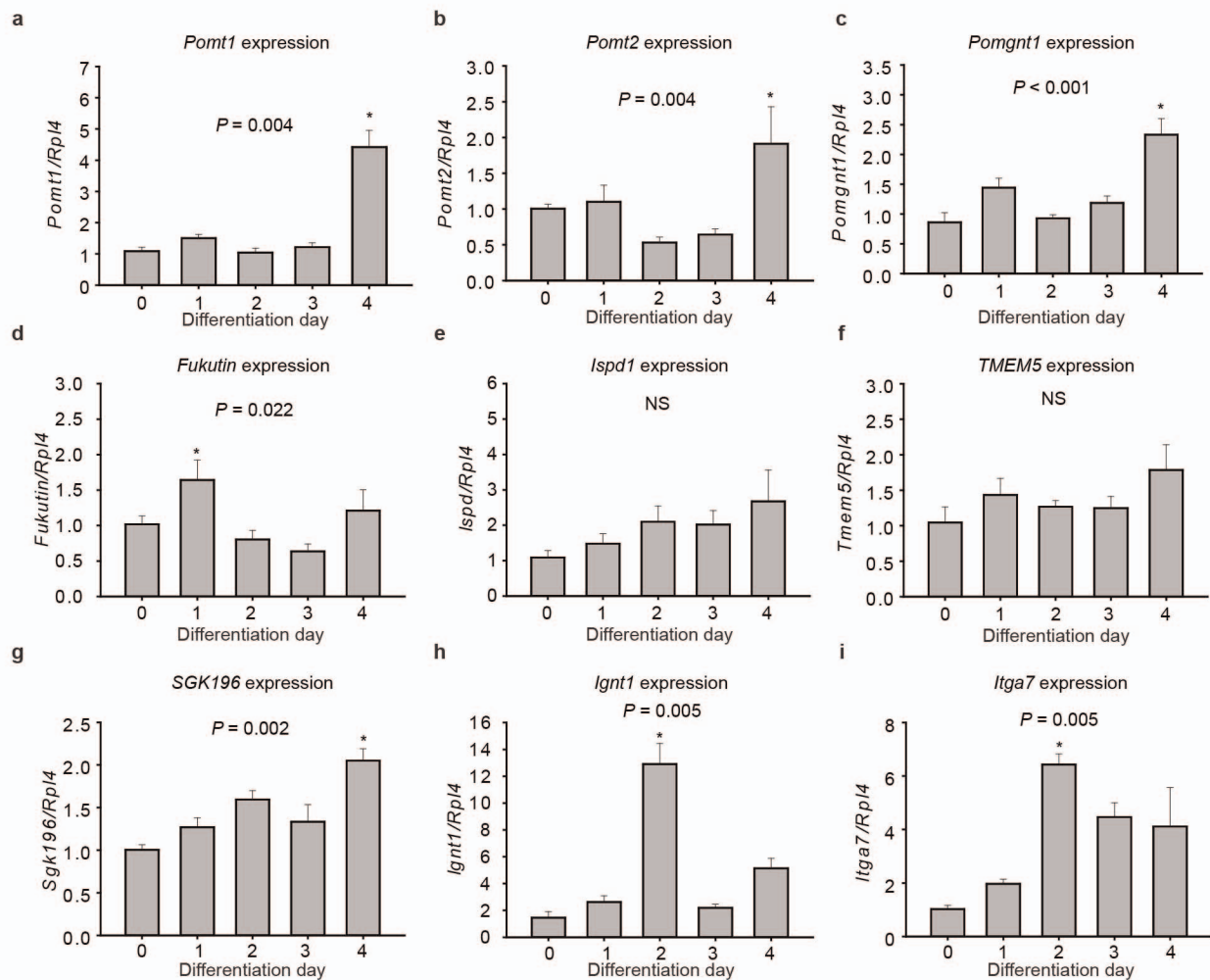
Extended Data Figure 4 | Expression analysis of *Large^{KD}* muscles undergoing regeneration. RT–PCR-based comparisons of gene expression in CTX and CL tibialis anterior muscles 10 days after injury, for *Large* (**a**), *Dag1* (**b**), collagen VIα (*Col6a*) (**c**), laminin α2 (*Lama2*) (**d**), laminin β1 (*Lamb1*) (**e**), perlecan (**f**) and agrin (**g**). $n \geq 3$ biological repeats and $n \geq 3$ technical repeats. The expression of all genes was compared to that for the reference gene *Rpl4*. Two-way ANOVA was used to analyse the data, and post-hoc comparisons between relevant groups are depicted; *$P < 0.05$, **$P < 0.001$, NS, not significantly different; error bars indicate s.e.m.
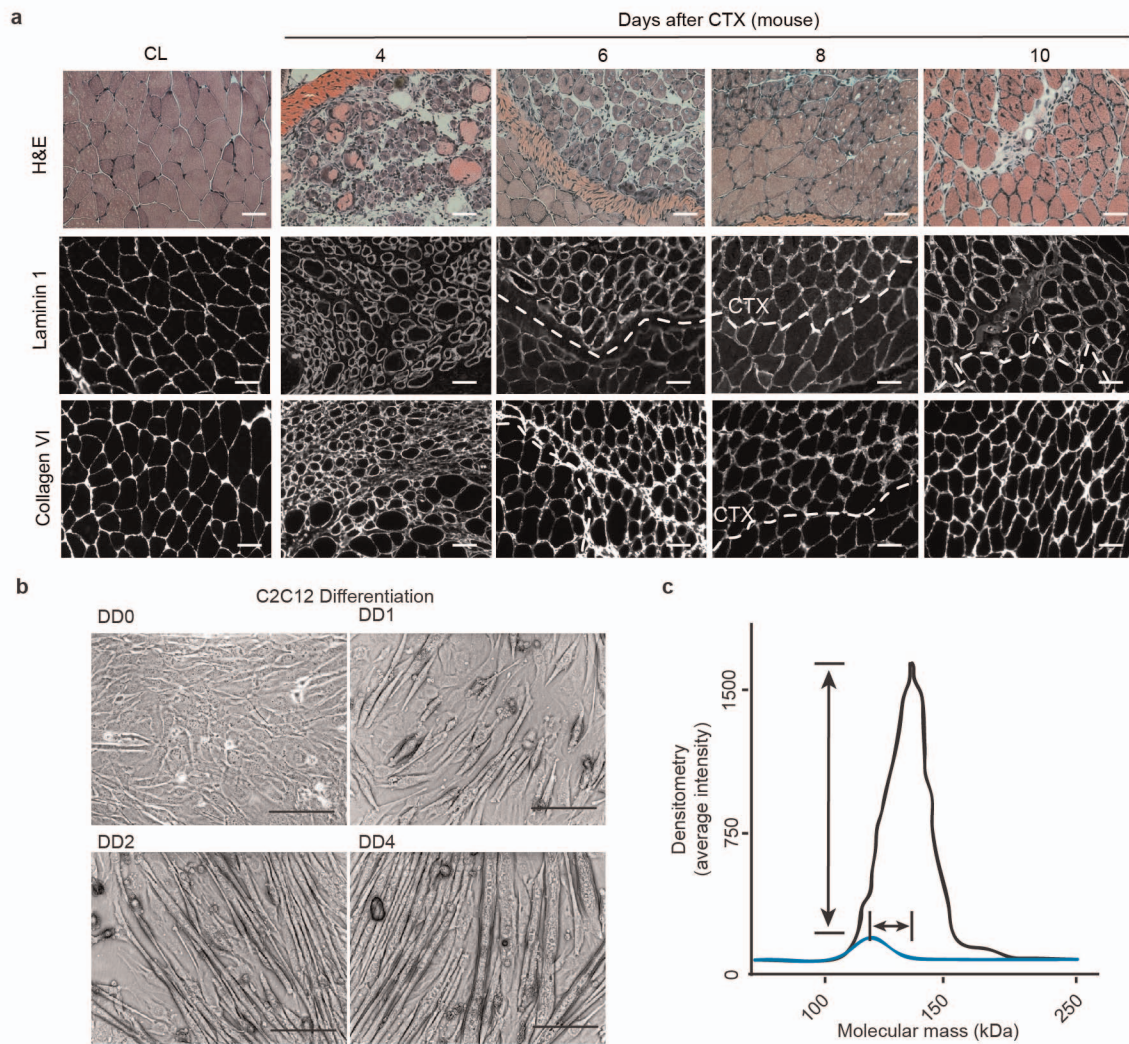
Extended Data Figure 5 | Muscle and basement membrane recovery from CTX injury and cellular hallmarks of C2C12 myogenesis. a, Serial sections of CTX-injected gastrocnemius muscle stained with haematoxylin and eosin (H&E) and with laminin and collagen antibodies. Existing laminin-containing basement membranes from degenerated myofibres are observable 4 days after CTX treatment. In areas of injury to myofibres (determined by central nucleation of myofibres), laminin and collagen VI are increased in intensity and appear more diffuse than in nearby uninjured regions. Dotted lines demarcate boundaries of damaged regions. Scale bars, 50 μm. CL, contralateral.

b, Confluent myoblast cultures stimulated to differentiate by switch to low-serum medium (viewed by phase contrast). Differentiation day (DD) 0 is defined as when C2C12 myoblasts reach confluence in growth medium. 24 h after switching to serum-restricted medium (DD1), the myoblasts are elongated and begin to align with one another. By DD2, myoblast fusion is apparent, and steady myotube growth is observed over the next several days. Scale bars, 100 μm. **c**, Representative densitometry-based quantification of IIH6-positive α-DG on DD0 (blue line) and DD5 (black).

Extended Data Figure 6 | Expression of α-DG-related genes during C2C12 myogenesis. qRT–PCR analysis for *Pomt1* (**a**), *Pomt2* (**b**), *Pomgnt1* (**c**), fukutin (**d**), *Ispd1* (**e**), *Tmem5* (**f**), *Sgk196* (**g**), *Ignt1* (**h**) and α7 integrin (*Itga7*, **i**) over the course of C2C12 myogenesis. Although significant changes in expression were observed for some genes, the pattern of expression did not match the increase in molecular mass observed in α-DG, or the increase observed in the expression of *Large* and *Dag1*. Biological and technical samples were assessed in triplicate. One-way ANOVA *P* values are included where significance was found, and time points with significantly increased expression (as determined by post-hoc analysis) are denoted with asterisks. *$P < 0.05$, NS, not significantly different; error bars indicate s.e.m.
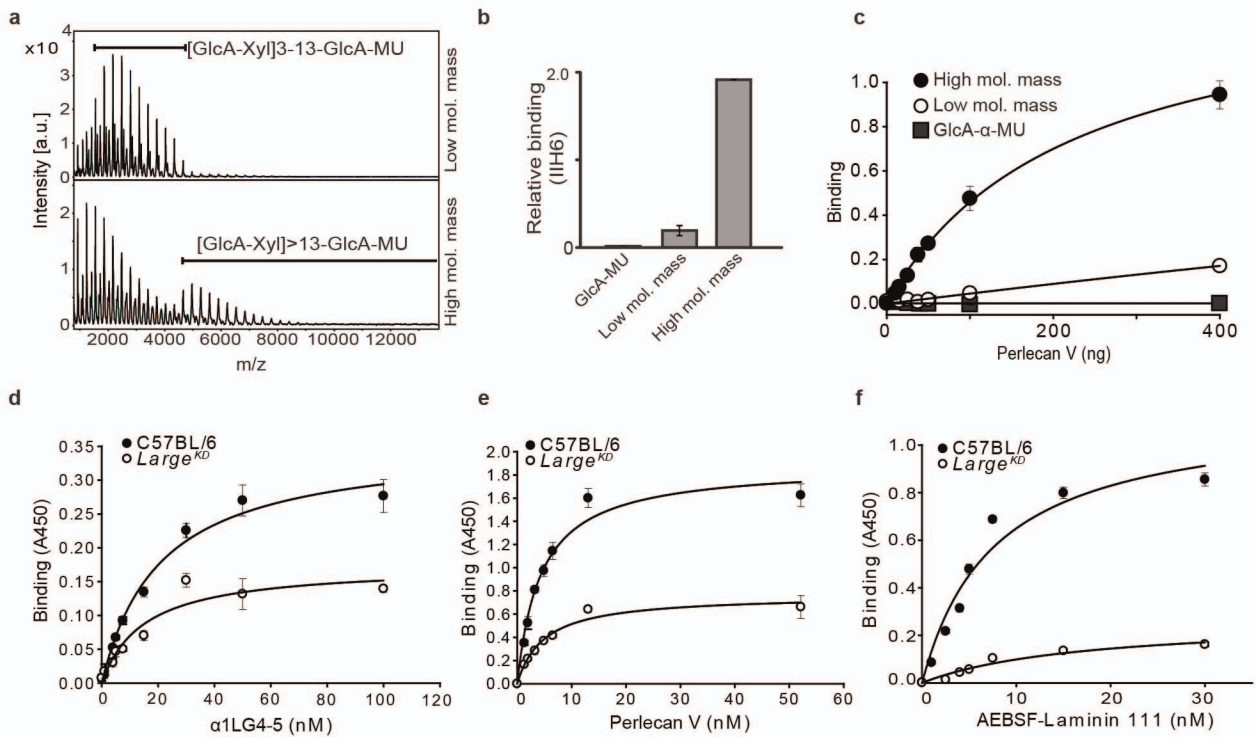
Extended Data Figure 7 | Mass spectrometry and binding characteristics of *in vitro* generated LARGE-glycan repeats and associated binding characteristics of *Large^KD* α-DG. a, Mass spectrometry analysis of high- and low-molecular-mass LARGE-glycan repeats using MALDI-TOF MS. High-molecular-mass species are under-represented owing to the difficulty in detecting polysaccharides of greater than 10 kDa using this approach[43]. **b**, IIH6 antibody binding to low- and high-molecular-mass LARGE-glycan repeats (error bars indicate s.e.m.). **c**, Solid-phase binding assay for the perlecan V domain (error bars indicate s.e.m.). **d**, Dystroglycan in DD4 myotubes generated from isolated primary *Large^KD* (+ 1 μg ml^{-1} doxycycline) and control satellite cells was assessed for substrate binding. Solid-phase α1LG4-5 binding demonstrated that binding capacity is dependent on extension of the LARGE-glycan (control $K_d = 15.0 \pm 5.20$ nM; *Large^KD* $K_d = 20.6 \pm 3.15$ nM). **e**, Findings for the perlecan V domain were similar to those of α1LG4-5 (control $K_d = 4.37 \pm 0.749$ nM; *Large^KD* $K_d = 4.88 \pm 0.846$ nM). **f**, Laminin 111 self assembles, and we wished to test the binding characteristics of a form that is unable to do so. AEBSF-laminin 111 is unable to polymerize yet retains receptor binding capacity[44] and when it was tested the differences in binding between *Large^KD* and control samples were greater than those for laminin 111. This finding indicates that the polymerization of laminin bound to LARGE-glycan reduces the apparent differences in binding between *Large^KD* and control α-DG (AEBSF-laminin 111 binding control $K_d = 7.61 \pm 2.12$ nM, $B_{max} = 1.14$; *Large^KD* $K_d = 17.1 \pm 7.36$ nM, $B_{max} = 0.268$). Error bars indicate s.e.m., curve fitting to equation $f = B_{max}*\text{abs}(x)/(K_d + \text{abs}(x))$.
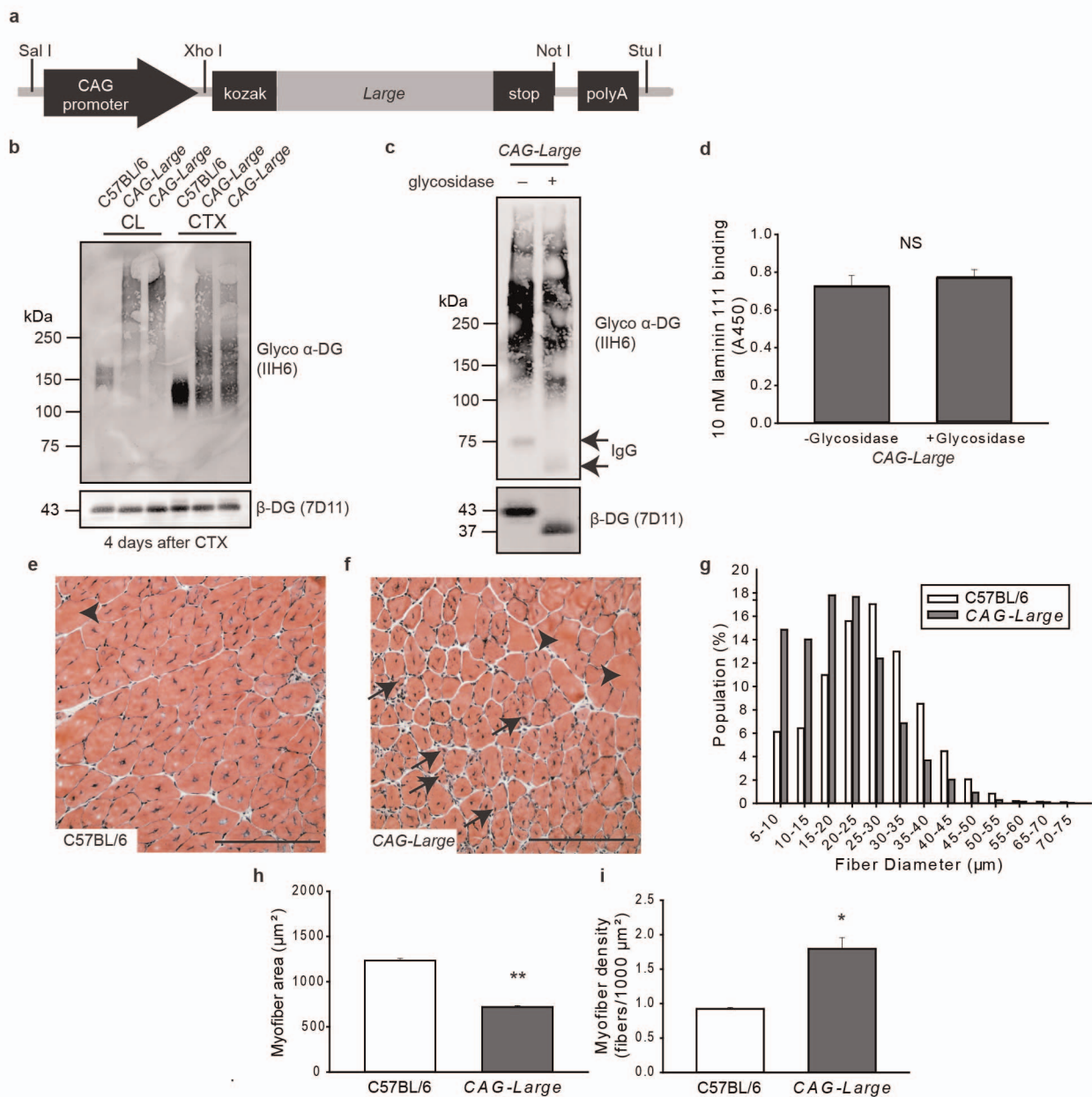
Extended Data Figure 8 | Overexpression of LARGE in a transgenic mouse results in abnormal muscle regeneration. a, Map of transgene used to generate the *CAG-Large* transgenic mouse. **b**, Western blot of α-DG from CL and CTX injured tibialis anterior muscles 4 days after injury, demonstrating that the protein is hyperglycosylated in *CAG-Large* muscles. **c**, WGA-enriched samples from *CAG-Large* muscles 10 days after CTX injury were treated with enzymatic de-glycosylation to remove *N*-glycans, certain α-DG mucin *O*-glycans and terminal trisaccharides of *O*-mannosyl tetrasaccharides while sparing the phosphorylated *O*-mannosyl-linked LARGE-glycan as evidenced by the maintenance of IIH6-positive α-DG and reduction in molecular mass of β-DG and the IgG present in the samples. **d**, No change in laminin 111 binding, as detected by solid-phase assay, was observed in glycosidase-treated *CAG-Large* samples (error bars indicate s.e.m., $n = 4$ biological replicates) compared to untreated samples indicating that despite *Large* overexpression, nonspecific LARGE modification is minimal in these muscles. **e**, **f**, Haematoxylin-and-eosin-based histological analysis of muscles 10 days after CTX injury revealed an increase in myofibres of small diameter, quantified in **g–i**. Scale bars represent 200 μm. >6,000 fibres per group were measured, $n = 3$ animals per group, *$P = 0.006$, **$P < 0.001$ by one-way ANOVA; error bars indicate s.e.m.
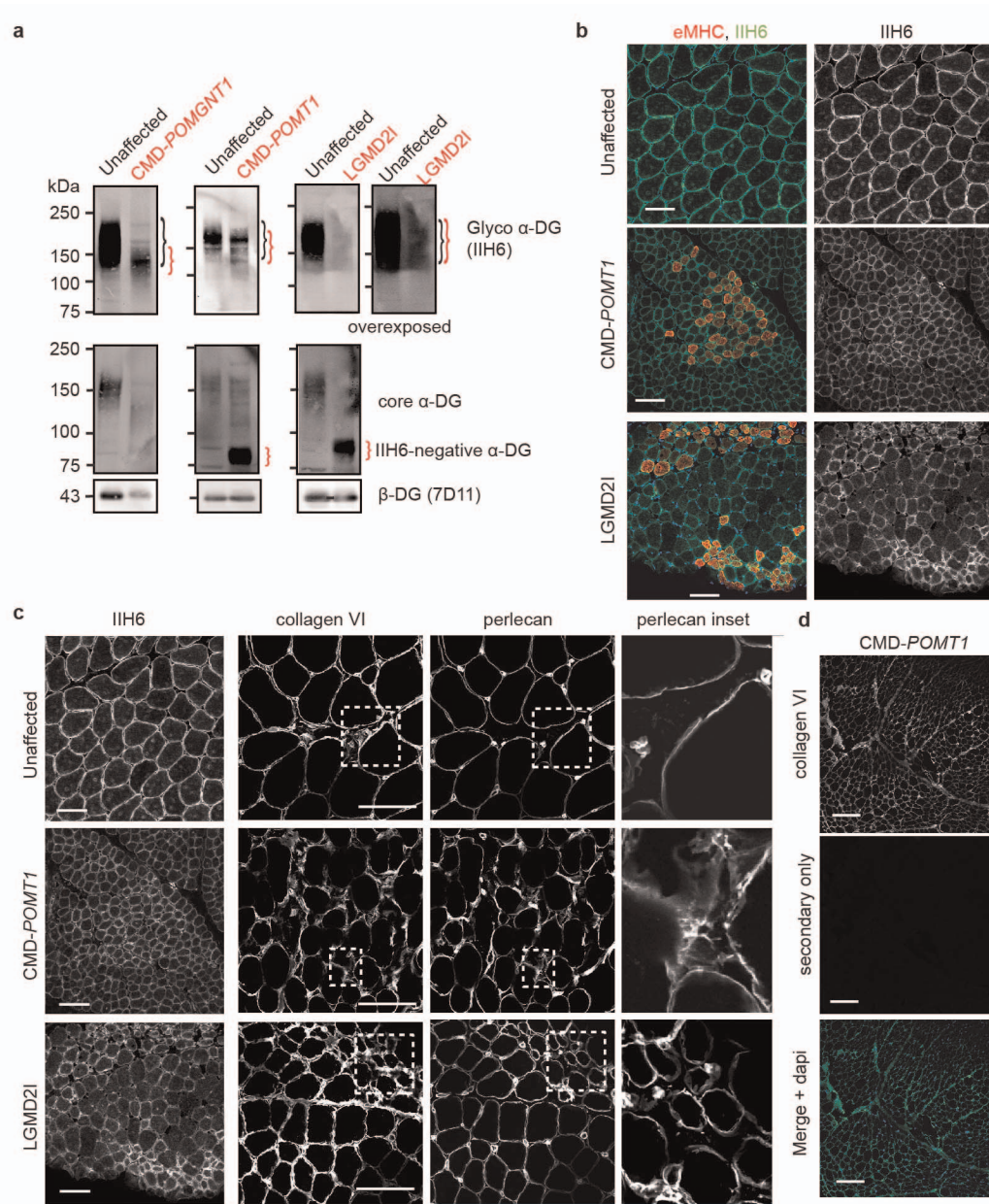
Extended Data Figure 9 | Increased IIH6 reactivity in regenerating myofibres from patients. a, Western blots of WGA-enriched muscle lysates from patient biopsies. CMD, congenital muscular dystrophy; LGMD2I, limb-girdle muscular dystrophy 2I. **b**, Patient biopsies were analysed by immunofluorescence for the presence of the α-DG LARGE-glycan (using antibody IIH6) and for signs of regeneration (using antibody to the embryonic myosin heavy chain, eMHC). Increased IIH6 signal correlates with regions of muscle regeneration. In the LGMD2I sample, IIH6 signal is nearly exclusively localized to regions of regeneration. **c**, Representative immunofluorescence images from patient muscle biopsies. Insets highlight mislocalized (endomysial) perlecan in CMD sample. Intense, localized capillary staining is also observed with perlecan antibody. **d**, Secondary only staining for perlecan in human dystrophic muscle sample, demonstrating that the signal in **c** is specific. Scale bars, 100 μm.
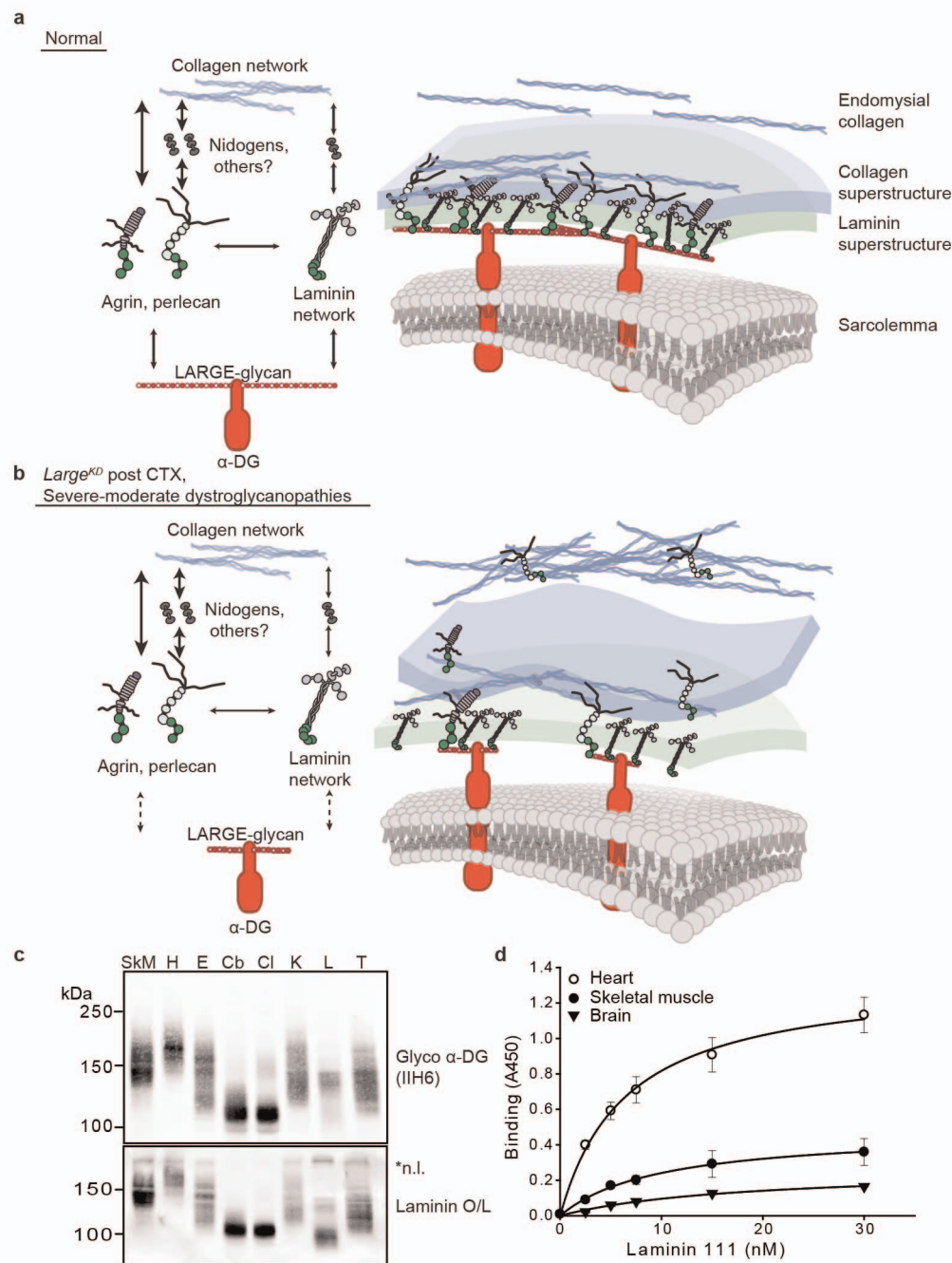
Extended Data Figure 10 | Model depicting the role of LARGE-glycan in organizing specialized basement membranes. a, In normal skeletal muscle, LARGE-glycan on α-DG is abundant and forms long chains, providing many binding sites for ligands such as laminin, agrin and perlecan. In addition to binding the LARGE-glycan, perlecan and agrin bind (directly, or indirectly via accessory proteins like nidogen) to laminin and collagen networks, providing collateral linkages as was recently suggested in regards to perlecan[45]. Increased collateral linkage probably enables compaction of the basement membrane. **b**, In *Large*[KD] muscle and some dystroglycanopathies, reduced extension of the LARGE-glycan during muscle formation results in a reduction in the number of binding sites for ligands, and the few collateral linkages between collagen, laminin and the sarcolemma are unable to compress the basement membrane. Also, because the basement membrane anchors less collagen, this protein accumulates in the endomysium where it provides ectopic binding sites for perlecan. Agrin is both a high-affinity ligand for the LARGE-glycan and highly concentrated at the NMJ. When the number of LARGE-glycan binding sites at the NMJ basement membrane is limited, agrin saturation of the NMJ may limit the laminin-mediated maturation of the NMJ[46]. Although DG is depicted as having only two LARGE-glycan chains in this model, it is likely that between 2 and 5 chains are present per DG molecule in skeletal muscle[7]. Integrins, which are not depicted here, can also bind laminin, and thus could contribute to this network; however, mouse studies indicate that its cellular roles are largely independent of DG[47]. **c**, Representative western blot analysis of α-DG in various mouse tissues, demonstrating extensive heterogeneity in molecular mass. Tissues were collected from C57BL6/J mice and samples from multiple mice were pooled before homogenization and Triton X-100 solubilization. Equal amounts of lysate, enriched for glycoprotein by WGA pull down, were loaded. Laminin 111 overlay assay demonstrated that despite differences in molecular mass, the α-DG glycoforms in various tissues retain the capacity to bind laminin. Cb, cerebrum; Cl, cerebellum; E, eye (globe); H, heart; K, kidney; L, lung; n.l., native laminin; SkM, skeletal muscle; T, thymus. **d**, However, higher molecular mass α-DG species have increased binding capacity for laminin 111, as demonstrated by solid-phase assay, indicating that tissue-specific modification of α-DG LARGE-glycan levels is a possible means to modify cell interactions with the extracellular matrix environment. Error bars indicate s.e.m., curve fitting to equation $f = B_{max}*abs(x)/(K_d + abs(x))$.